Palaeogeography, Palaeoclimatology, Palaeoecology xxx (2015) xxx–xxx

Contents lists available at ScienceDirect

Palaeogeography, Palaeoclimatology, Palaeoecology

journal homepage: www.elsevier.com/locate/palaeo

A multi-proxy approach to decode the end-Cretaceous mass extinction

Jahnavi Punekar [a,*], Gerta Keller [a], Hassan M. Khozyem [b], Thierry Adatte [c], Eric Font [d], Jorge Spangenberg [c]

[a] Geosciences, Princeton University, Princeton, NJ 08540, USA
[b] Department of Geology, Faculty of Science, Aswan University, Aswan 81528, Egypt
[c] Institute of Earth Sciences, University of Lausanne, 1015 Lausanne, Switzerland
[d] IDL-FCUL, Instituto Dom Luís, Faculdade de Ciências, Universidade de Lisboa, Portugal, Campo Grande, 1749-016, Lisbon, Portugal

ARTICLE INFO

Article history:
Received 17 January 2015
Received in revised form 9 July 2015
Accepted 19 August 2015
Available online xxxx

Keywords:
Low magnetic susceptibility
Planktic foraminifera
Carbonate-dissolution
Ocean acidification
Deccan volcanism

ABSTRACT

Mass extinctions generally involve a complex array of interrelated causes and are best evaluated by a multi-proxy approach as applied here for the end-Cretaceous mass extinction. This study documents and compares the planktic foraminiferal records, carbonate dissolution effects, stable isotopes, and magnetic susceptibility in France (Bidart), Austria (Gamsbach) and Tunisia (Elles) in order to explore the environmental conditions during the uppermost Maastrichtian *Plummerita hantkeninoides* zone CF1 leading up to the mass extinction. Planktic foraminiferal assemblages at Bidart and Gamsbach appear to be more diverse than those at Elles, with unusually high abundance (20–30%) and diversity (~15 species) of globotruncanids in the two deep-water sections but lower abundance (<10%) and diversity (<10 species) at the middle shelf Elles section. Oxygen isotopes in zone CF1 of Elles record rapid climate warming followed by cooling and a possible return to rapid warming prior to the mass extinction.

The onset of high stress conditions for planktic foraminifera is observed ~50–60 cm below the KTB at Bidart and Gamsbach, and ~4.5 m below the KTB at Elles due to much higher sediment accumulation rates. These intervals at Bidart and Gamsbach record low magnetic susceptibility and high planktic foraminiferal fragmentation index (FI) at Elles, Bidart and Gamsbach. An increased abundance of species with dissolution-resistant morphologies is also observed at Gamsbach. The correlative interval in India records significantly stronger carbonate dissolution effects in intertrappean sediments between the longest lava flows, ending with the mass extinction. Based on current evidence, this widespread dissolution event stratigraphically coincides with the climate cooling that follows the Late Maatrichtian global warming and may be linked to ocean acidification due to Deccan volcanism. The estimated 12,000–28,000 Gigatons (Gt) of CO_2 and 5200–13,600 Gt of SO_2 introduced into the atmosphere likely triggered the carbonate crisis in the oceans resulting in severe stress for marine calcifiers leading to mass extinction.

1. Introduction

One of the best-known European Cretaceous–Tertiary boundary (KTB) sections, also known as Cretaceous–Paleogene (KPB or KPg) sections, is exposed at a beach near Bidart in the Basque–Cantabrian basin of southwestern France (Figs. 1, 2B, Seyve, 1990; Haslett, 1994). At this locality, about 8 m of uppermost Maastrichtian and ~4 m of basal Danian sediments are exposed including the boundary clay, an Iridium (Ir) anomaly and negative $\delta^{13}C$ excursion that indicate a relatively complete KTB transition (Fig. 2A, C; Renard et al., 1982; Bonté et al., 1984; Apellaniz et al., 1997; Font et al., 2014). Nevertheless, the Bidart section remained in limbo for nearly two decades because of uncertain age control, particularly the reported absence of the latest Maastrichtian nannofossil *Micula prinsii* zone and absence of the planktic foraminiferal zones CF1 (*Plummerita hantkeninoides*) and CF2, which together are correlative with paleomagnetic chron C29r. This led to the assumption that the latest Maastrichtian is missing (Gallala et al., 2009). Subsequent paleomagnetic and microfossil studies revealed that the ~8 m of uppermost Maastrichtichtian sediments below the KTB were deposited during the *Micula prinsii* zone (Galbrun and Gardin, 2004) and the recent finding of *P. hantkeninoides* zone CF1 (Font et al., 2014) further confirms deposition in paleomagnetic chron C29r below the KTB boundary and hence a substantially complete KTB transition.

Restudy of the Bidart section is particularly important because of the potential connection between the high-stress interval spanning the last 50-cm of the Maastrichtian and Deccan volcanism in India (Font et al., 2011, 2014). As early as in the 1990s, Apellaniz et al. (1997) reported a drop in carbonate content and increased planktic foraminiferal test dissolution particularly in the KTB clay and the underlying 28-cm of uppermost Maastrichtian sediments. This interval depleted in carbonate content is also featured by a loss of iron oxides (biogenic and detrital magnetite), interpreted to be the result of acidification linked to Deccan acid rains (Font and Abrajevitch, 2014; Font et al., 2014). The possible

* Corresponding author. Tel.: +1 609 258 6482.
E-mail address: jpunekar@princeton.edu (J. Punekar).

http://dx.doi.org/10.1016/j.palaeo.2015.08.025
0031-0182/

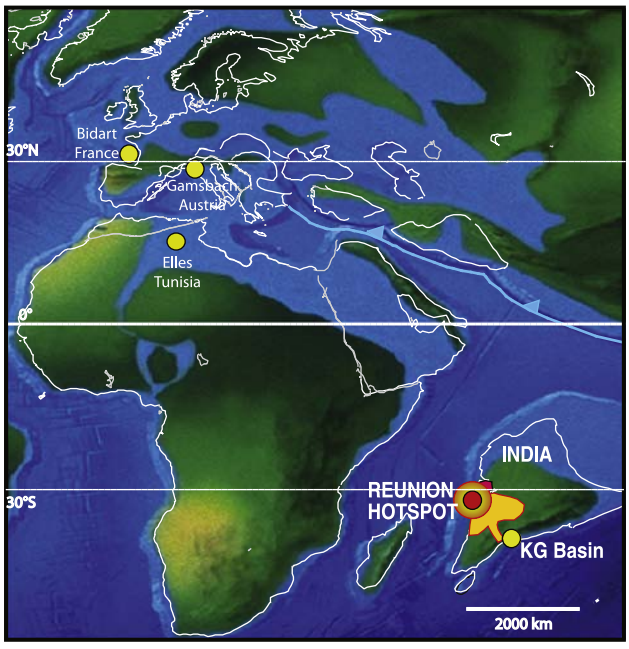

Fig. 1. Palaegeographic map of 66 Ma showing the study sections Bidart (France) and Gamsbach (Austria) and the reference section Elles (Tunisia, GSSP) relative to the location of the Reunion hotspot (focal point of Deccan volcanism). Modified after ©2000 C R Scotese PALEOMAP Project.

link between this dissolution interval and ocean acidification related to Deccan volcanism appears to be more than coincidental and warrants a fresh investigation of associated changes in planktic foraminiferal assemblages. Bidart therefore provides a unique opportunity to analyze this critical time interval in Earth history to understand the environmental changes in the northern mid-latitude Atlantic Ocean that may be related to the global effects of Deccan volcanism.

Preliminary faunal analysis of the Bidart section reveals a planktic foraminiferal assemblage remarkably different from those reported for El Kef (GSSP) and Elles, Tunisia, and other continental shelf locations (Abramovich and Keller, 2002; Font et al., 2014). To evaluate whether this is due to different depositional settings (open ocean bathyal depths for Bidart versus shelf depth for Tunisia), we chose a second bathyal section, Gamsbach, Austria, as a control site. Gamsbach is located in the Eastern Alps with a palaeogeographic setting and depositional history similar to Bidart (Figs. 1, 3B; Grachev et al., 2005). Gamsbach contains planktic foraminiferal assemblages similar to those at Bidart, including a pre-KTB dissolution interval that supports the choice of Gamsbach as a complementary site.

Although numerous studies have explored the KTB transition at Bidart and Gamsbach over the past three decades (see sections 1 and 2, supplementary material), the published microfossil records are generally not quantitative and at very low sample resolution yielding little or no information for the critical pre-extinction interval. We present comprehensive biostratigraphic, assemblage and stable isotope, geochemical and mineralogical data that focus on the rapid climatic and biotic events of zone CF1, which globally record the crises that led up to the KTB mass extinction. The primary objective of this study is to test the hypothesis that Deccan volcanism may have caused global climate changes and ocean acidification that directly resulted in the KTB mass extinction recorded in planktic foraminifera.

We test this hypothesis based on: (1) High-resolution quantitative planktic foraminiferal species abundances through the uppermost Maastrichtian zones CF1–CF2 at Bidart and Gamsbach; (2) high-resolution biostratigraphic analysis with special emphasis on the presence/absence of index species (e.g., *Gansserina gansseri* and *Plummerita hantkeninoides*) to re-evaluate the conflicting published reports (reviewed below); (3) evaluation of the palaeoclimatic and the paleoenvironmental conditions recorded in stable isotopes, geochemical proxies, and associated biotic events; (4) evaluation of carbonate and iron oxide dissolution events based on the quality of foraminiferal test preservation (fragmentation index FI) and magnetic susceptibility, respectively; (5) determination of the chronologic sequence of biotic, climatic and geochemical events through zone CF1 at Bidart and Gamsbach, as well as their regional and global oceanographic significance in the context of environmental perturbations related to Deccan volcanism; and (6) comparison with shelf sequences at Elles and El Kef, Tunisia, to assess the nature of environmental changes in shallow vs. deep-water environments.

2. Background

2.1. Bidart and Gamsbach

Previous studies of the Bidart and Gamsbach sections report sedimentologic, geochemical, paleomagnetic and microfossil biostratigraphic data. A brief summary is presented here (see supplementary material for details).

2.1.1. Bidart

Planktic foraminifera and nannofossils record a rapid decline at the KTB in Bidart (Gorostidi and Lamolda, 1995; Apellaniz et al., 1997; Thibault et al., 2004; Gallala et al., 2009), whereas benthic foraminifera switch from infaunal to epifaunal dominance across the KTB (Alegret et al., 2004). An Iridium anomaly of 6.3 ± 1.1 ppb, enrichment of Co, Cr, Ni, As, Sb, and Se, and depletion of rare earth elements (REE) are reported in the Bidart KTB red clay layer (Delacotte, 1982; Smit and Ten Kate, 1982; Bonté et al., 1984). Some studies report the presence of microtektites, microspherules and Ni-rich crystals in the KTB red layer in the Basque sections but provide no supporting data (Apellaniz et al., 1997; Arz and Arenillas, 1998; Arenillas et al., 2004).

2.1.2. Gamsbach

Previous studies on Gamsbach show the KTB clay enriched in Ir (6 ppb), iron hydroxides, Co, Ni, Cr and siderophile elements and sporadic occurrence of pure Ni crystals, awaruite (Fe_3Ni), Ni–Fe, Ni–Fe–Mo and Ni–Fe–Co alloys, cosmic dust and spherules of varied geochemical affinities (Grachev et al., 2005, 2008; Pechersky et al., 2006; Egger et al., 2009). Micropaleontological and biostratigraphic studies are limited due to poor carbonate preservation throughout the KTB transition (Egger et al., 2004, Summesberger et al., 2009, Korchagin and Kollmann in Grachev, 2009). Summesberger et al. (2009) reported on the cephalopod, nannofossil and planktic foraminiferal biostratigraphy at Gamsbach but provided no quantitative documentation.

2.2. Deccan volcanism

Deccan eruptions resulted in an estimated 1.5 million km^3 of lava flooding the Indian sub-continent (Raja Rao et al., 1999). Three main phases of eruptions are recognized: the initial phase-1 (~6% of the total volume) in the early late Maastrichtian recently dated by $^{40}Ar/^{39}Ar$ at 67.12 ± 0.44 Ma at the chron C30n/C29r transition (Schöbel et al., 2014); the main phase-2 (~80% of the total lava pile) in chron C29r (Subbarao et al., 2000; Chenet et al., 2007, 2008; Jay and Widdowson, 2008; Schoene et al., 2014) culminating in the KTB mass extinction (Keller et al., 2011a, 2012); and the final phase-3 (~14% of the total volume) in the early Danian chron C29n. The environmental effects of the three Deccan phases are determined by the tempo and magnitude of eruptions and the amounts of SO_2, CO_2, Cl and other gases released into the atmosphere (Self et al., 2008). A global review of the planktic foraminiferal events contemporaneous with Deccan phase-2 and phase-3 can be found in Punekar et al. (2014a).

Please cite this article as: Punekar, J., et al., A multi-proxy approach to decode the end-Cretaceous mass extinction, Palaeogeogr. Palaeoclimatol. Palaeoecol. (2015), http://dx.doi.org/10.1016/j.palaeo.2015.08.025

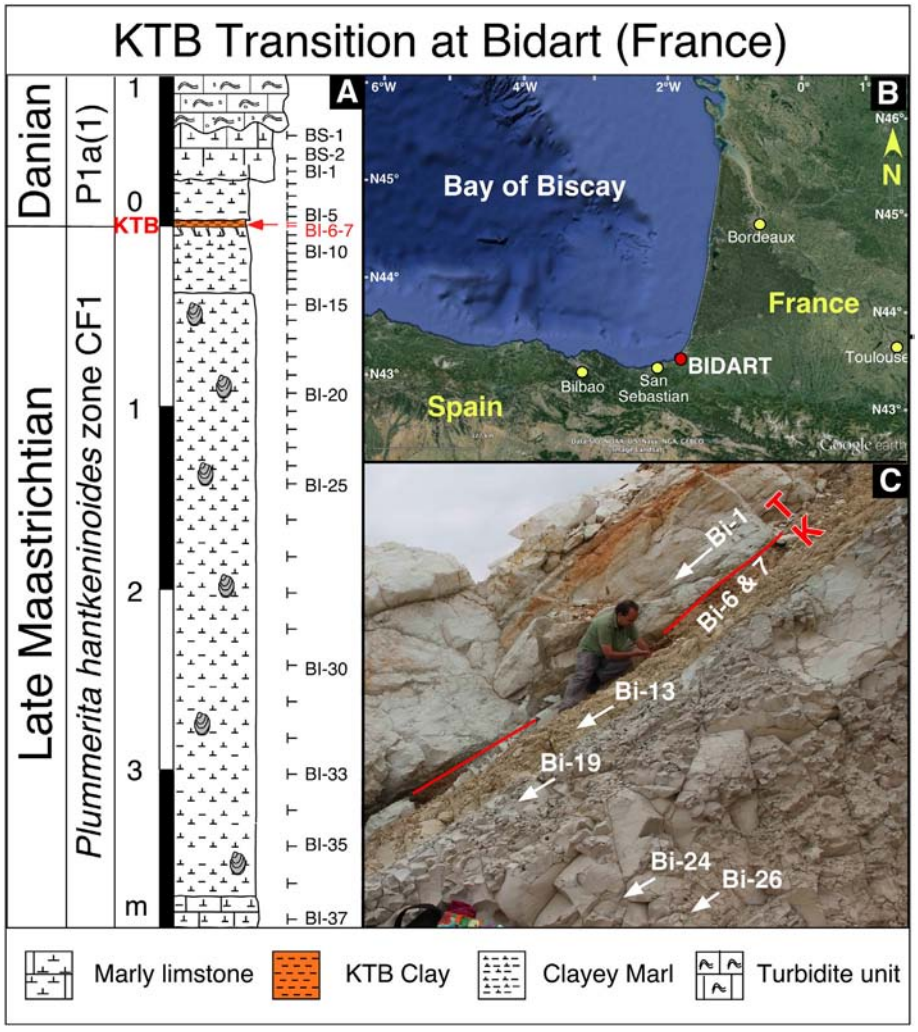

Fig. 2. (A) Lithological log of the upper Maastrichtian-basal Danian interval studied at Bidart, the red layer marks the KTB (B) Google Earth image showing the present day location of Bidart (C) Field photograph of the Bidart section showing the sampled interval and the position of KTB (in red). (For interpretation of the references to color in this figure legend, the reader is referred to the web version of this article.)

In the Krishna–Godavari Basin of SW India a rapid succession of four phase-2 lava mega-flows span C29r below the KTB and mark the CF1–CF2 and *Micula prinsii* (nannofossil) zones; intertrappean sediments reveal rapid extinctions (Keller et al., 2011a, 2012). The correlative interval in Meghalaya (NE India) is dominated (95%) by *Guembelitria* blooms, and high-stress is also marked by ocean acidification and strong carbonate dissolution (Gertsch et al., 2011). Schoene et al. (2014) show that the Phase-2 volcanism itself lasted ~500-kyr into the Danian. On a global basis paleoclimatic data from DSDP Site 525A (Li and Keller, 1998a), Tunisia, (Stüben et al., 2003) and Texas (Abramovich et al., 2011; Keller et al., 2011b) show at least one and possibly multiple hyperthermal events during the CF1–CF2 global warming, which indicates complex and episodic climate fluctuations in the latest Maastrichtian correlative with Deccan phase-2 (Punekar et al., 2014a).

At Bidart and Gubbio Font et al. (2011, 2014) discovered akaganeite, an unusual Cl-bearing iron hydroxide preserved in a low magnetic susceptibility (MS) interval below the KTB. The origin of this low MS interval is explained by the loss of detrital and biogenic magnetites from reductive iron hydroxide dissolution due to acid rains and ocean acidification linked to Deccan Phase-2 (Font et al., 2014). They proposed a Deccan volcanic origin for akaganeite, formed by interaction of acid aerosols with the high atmosphere and potentially transported through the stratosphere at Bidart (Atlantic realm) and Gubbio, Italy (Tethys realm). If a volcanic origin for akaganeite is confirmed, this can provide a promising new geochemical benchmark for identifying Deccan environmental effects across the globe.

3. Geologic setting and lithology

3.1. Bidart, France

The Bidart KTB boundary section outcrops along the Erreteguia beach 2 km north of Bidart and can be accessed by the national highway R.N. 10 (W 1°35′, N 43°26′; Fig. 2B). Sediments consist of hemipelagic to pelagic marls and limestones deposited at upper-middle bathyal depths in the Aturian Trough during the late Maastrichtian to Paleocene (Alegret et al., 2004; Galbrun and Gardin, 2004; Font et al., 2011). Deposition occurred in a flysch zone and accumulated at 3–4 cm/ky, resulting in thick marl beds (Seyve, 1984; Nelson et al., 1991; Clauser, 1994; Peybernes et al., 1997; Vonhof and Smit, 1997). Tectonic disturbance (Pyrenean orogeny) and diapirism resulted in interbed sliding, slickensides, and mass-flow deposits (Razin, 1989; Apellaniz et al., 1997).

About 8 m of uppermost Maastrichtian (C29r) pink to purple marlstones and marls with occasional turbidites and cut by local faults are exposed below the KTB at Bidart and can be traced throughout the Basque basin (Fig. 2A; Apellaniz et al., 1997). At the base of the section analyzed is a 25-cm thick marlstone followed by ~2.5 m of marls with common pelecypod shells and fragments. In the ~50-cm below the KTB, carbonate content decreases and macrofossils are absent, except

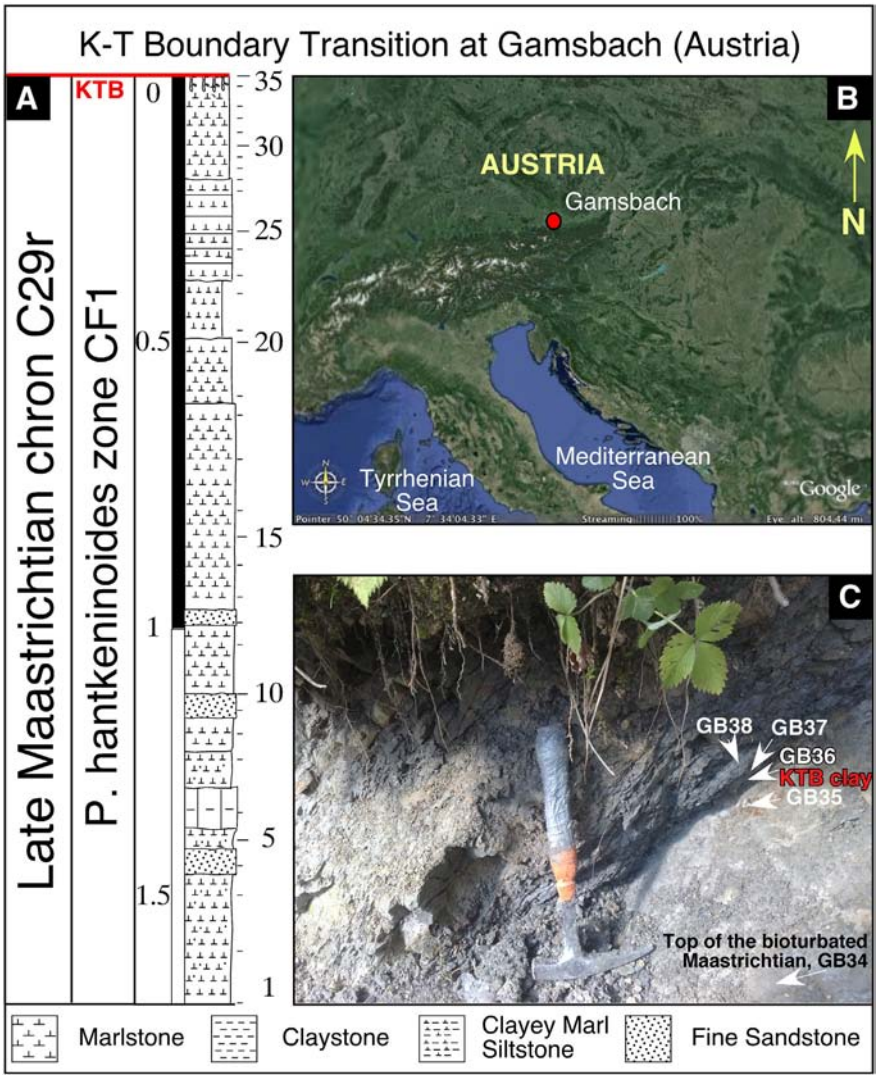

Fig. 3. (A) Lithological log of the uppermost Maastrichtian interval of Gamsbach, the red layer marks the KTB (B) Google Earth image showing the present day location of Gamsbach (C) Field photograph of the Gamsbach section showing the position of KTB (in red). (For interpretation of the references to color in this figure legend, the reader is referred to the web version of this article.)

at the top of this interval where burrows are truncated by the overlying boundary clay.

The KTB is easily recognized by a 2 mm "rusty" layer at the base of an 8–15 cm thick clay layer (Fig. 2B, C; Bonté et al., 1984; Apellaniz et al., 1997). The base of the clayey interval is a gray to yellow silty clay overlain by red brown siltstone and a thinly laminated dark gray siltstone at the top. Carbonate content gradually increases in the overlying basal Danian claystones, which are overlain by hemipelagic limestones marked by alternating pink and white (occasionally glauconitic) biogenic limestones bioturbated near the top of the section (Apellaniz et al., 1997; Font et al., 2011). At the top of the outcrop is a mass-flow deposit with an erosive basal surface.

3.2. Gamsbach, Austria

The KTB section is located in the Gamsbach valley of the Austrian Alps (E 14°51′50; N 47°39′51; Fig. 3B). During the KTB transition the Gamsbach area was located in the northwestern Tethys between paleolatitudes 20° to 30°N (Fig. 1; Haubold et al. 1999; Pueyo et al. 2007). The basin was formed after the early Cretaceous thrusting, followed by transtension and subsidence due to subduction (Wagreich, 1993, 1995). Erosion at the front of the Austro-Alpine microplate resulted in deposition of sediments at middle bathyal depths (600–1000 m) during the late Maastrichtian and lower bathyal depth (>1000 m) in the early Danian (Egger et al., 2009).

Sediments consist of hemipelagic pelites interbedded with thin sandy turbidites (<15 cm) characteristic of the Nierental Formation of the Gosau group in the northern calcareous Alps (Wagreich and Krenmayr, 1993, 2005). The Maastrichtian is composed of medium gray marlstones and marly limestones. Truncated burrows mark the top of the Maastrichtian below the 2-cm thick clay layer that marks the KT boundary. This KTB clay layer contains 0.2–0.4 cm thick yellowish clay at the base (Fig. 3A, C).

4. Material and methods

Sampling at Bidart concentrated on the 3.5 m interval below the KTB with samples collected at 15-cm intervals for the bottom 3 m and 5-cm intervals for the top 50-cm. At Gamsbach, 2 m of the uppermost Maastrichtian below the KTB were sampled at 5–6 cm intervals. In the laboratory, samples were crushed into small fragments and left overnight in 3% hydrogen peroxide solution to oxidize any organic carbon. The disaggregated sediment samples were then washed through >63 μm and >38 μm sieves (Keller et al., 1995). The washed residues were oven dried at 50 °C. Quantitative faunal analysis was based on 63–150 μm and >150 μm size fractions. Each size fraction of every

Please cite this article as: Punekar, J., et al., A multi-proxy approach to decode the end-Cretaceous mass extinction, Palaeogeogr. Palaeoclimatol. Palaeoecol. (2015), http://dx.doi.org/10.1016/j.palaeo.2015.08.025

sample was split with an Otto micro-splitter to obtain approximately 300 specimens of planktic foraminifera (for a statistical representation of the species population). These were picked, sorted and mounted on micro-slides and identified. The residual sample was searched for rare species and index species for biostratigraphy but not included in the quantitative dataset. Species identification is based on standard taxonomic concepts (e.g., Robaszynski et al., 1983–1984; Nederbragt, 1991; Olsson et al., 1999).

For the foraminifera fragmentation index, a microsplitter was used to obtain approximately 500–700 foraminifera and fragments from the >63 μm fraction such that at least 100 entire tests were counted. Three categories were identified based on the quality of preservation: entire (nearly) perfect tests (Plate 1, Plate 3: A–G), partially damaged (imperfect) tests (Plate 2: A–L; Plate 3: H–L, O, P) and fragments (Plate 2: M–T; Plate 3: M, N, Q–S). Specimens consisting of less than two-third of an entire test were counted as fragments (Berger et al., 1982). Planktic foraminifera fragmentation data was obtained for Bidart, Gamsbach and Elles sections. Benthic foraminifera fragmentation data was also obtained for Bidart to account for mechanical breakage due to post-depositional transport and sample processing techniques.

Stable carbon and oxygen isotope analyses were performed on whole-rock samples from Gamsbach for this study. These analyses were conducted using a Thermo Fisher GasBench II preparation device interface with a Thermo Fisher Delta Plus XL continuous flow isotope ratio mass spectrometer at the Institute of Earth Surface Dynamics (IDYST) of the University of Lausanne, Switzerland. The stable carbon and oxygen isotope ratios are reported in delta (δ) notation as permil (‰) deviation relative to the Vienna Pee Dee belemnite (VPDB). Whole rock and clay mineral data were acquired from XRD analyses using SCINTAG XRD 2000 Diffractometer at the Geological Institute of the University of Lausanne, Switzerland. The procedure for sample processing was based on Adatte et al. (1996).

Mass specific magnetic susceptibility (MS) was measured at the Institute Dom Luís (IDL), at the University of Lisbon, Portugal with a MFK-1 (AGICO). Rock fragments were crushed by using an agate mortar and filled within typical cubic plastic boxes of 8 cm^3 in volume. MS values are reported relative to mass (m^3/kg).

5. Biostratigraphy: how complete is the KTB transition?

To evaluate the stratigraphic completeness of the KTB transition we apply the high-resolution planktic foraminiferal zonal scheme by Li and Keller (1998a, 1998b) and Keller et al. (1995, 2002a) (Fig. 4). The KTB is placed at 65.5 Ma (Gradstein et al., 2004). However, the precise age of this boundary event is in flux with more recent geochronologic dating suggesting an age closer to 66.0 Ma (Renne et al., 2013) and additional dating still in progress. Based on cyclostratigraphy the duration for paleomagnetic chron C29r is estimated at 750 ky with the base of C29r at 66.25 Ma (Gradstein et al., 2004; Schoene et al., 2014; Thibault and Husson, in press).

5.1. Uppermost Maastrichtian Zone CF1

This zone is defined by the total range of the index species *P. hantkeninoides*. Previous studies concluded that *P. hantkeninoides* is absent at Bidart (Arz and Molina, 2002; Gallala et al., 2009; Gallala, 2013). However, we observed this species in the 5 m below the KTB (see also Font et al., 2014) and 1.75 m below the KTB at Gamsbach (Supplementary material Section 3). This indicates that in both localities the uppermost Maastrichtian zone CF1 is present. Zones CF1 and CF2 are equivalent to the upper part of the nannofossil *M. prinsii* zone, which spans the top 8 m of the Bidart section (Galbrun and Gardin, 2004) and corresponds to C29r below the KTB. The sediment accumulation rate for this interval is 3.2 cm/ky (800 cm/250 ky) and 3.1 cm/ky for zone CF1. Previous studies estimated a sedimentation rate of 4 cm/ky for the Maastrichtian distal sea fan at Bidart (Seyve, 1990; Nelson et al., 1991; Vonhof and Smit, 1997) and 2.5 cm/ky for the nearby Sopelana section (Mary et al., 1991). This study suggests that the zone CF1 interval is substantially complete, although truncated burrows at the top of CF1 just below the KT boundary clay suggest some erosion. Compared with the middle bathyal environment at Bidart, the middle shelf depositional environment at Elles, Tunisia, reveals a much higher sediment accumulation rate of 8.6 cm/ky for C29r below the KTB. Based on this section, the duration of zone CF1 is estimated at ~160 ky based on the KTB at 65.5 Ma (Gradstein et al., 2004). Considering the KTB at 66 Ma and the C30n/C29r transition at ~66.288 Ma, zone CF1 at Elles is ~130 ky long (Renne et al., 2013; Schoene et al., 2014)

At Gamsbach, *P. hantkeninoides* was identified in the top ~1.75 m of the Maastrichtian for the first time in this study (Fig. 6B, Plate 1: M). Truncated burrows mark the top of zone CF1 below the boundary clay similar to Bidart. Based on these observations we conclude that the upper part of zone CF1 to the KTB mass extinction at Gamsbach is similar to Bidart and substantially complete. The abrupt negative $\delta^{13}C$ shift in bulk rock at the KTB and the presence of an erosional surface truncating burrows at both Gamsbach and Bidart suggests some erosion. Biostratigraphy indicates that erosion was primarily of basal Danian sediments.

5.2. KT boundary clay zone P0

The KTB consists of a "boundary clay" zone P0 overlying the Maastrichtian mass extinction horizon. The boundary is easily identified on the basis of five globally verified criteria: (1) mass extinction of Cretaceous planktic foraminifera, (2) appearance of the first five Danian species within a few cm of the boundary clay, (3) KTB clay and red layer, (4) an Ir anomaly and (5) the $\delta^{13}C$ negative shift (Keller et al., 1995, 2011b). The KTB is also characterized by an abrupt increase in magnetic susceptibility (Font et al., 2011; this study). At Bidart and Gamsbach, the KTB clay is very thin (~5 cm and ~3 cm respectively) and overlies an erosion surface with truncated burrows. The zone P0 clay, which is defined by the interval between the mass extinction horizon and first appearance of *Parvularugoglobigerina eugubina*, is absent as this species directly overlies the mass extinction horizon. Ir anomalies of 6.3 ppb and ~6.0 ppb at Bidart and Gamsbach, respectively (Bonté et al., 1984; Vonhof and Smit, 1997; Egger et al., 2009) are concentrated in the thin clay that represents redox conditions above the erosion surface. Similarly, the $\delta^{13}C$ negative shift of 2.0 to 2.3‰ is abrupt across the erosion surface in both sections (Rocchia et al., 1987; Font et al., 2014). In comparison, at the stratotype El Kef and expanded Elles sections in Tunisia, the P0 clay is 50 to 75 cm thick with an Ir anomaly of 18 ppb at the base and a 4‰ negative carbon isotope excursion (Rocchia et al., 1996; Stüben et al., 2003). The relative time represented by the condensed P0 intervals and hiatuses at Bidart and Gamsbach can be estimated based on the zone P1a planktic foraminiferal assemblages.

5.3 . Zone P1a hiatuses

This zone is defined by the total range of *P. eugubina* and/or *P. longiapertura* and can be subdivided into subzones P1a(1) and P1a(2) based on the FO of *Parasubbotina pseudobulloides* and/or *Subbotina triloculinoides* (Fig. 4). At the time of the P0/P1a(1) boundary only about five early Danian species had evolved and all were rare as the assemblages were dominated by the Cretaceous survivor and disaster opportunists *Guembelitria* species (review in Keller and Pardo, 2004).

At Bidart, zone P1a(1) directly overlies the mass extinction with common *Parvularugoglobigerina extensa*, *P. eugubina* and *P. longiapertura*, an assemblage that is known to first appear well into zone P1a(1) about 100 kyr after the KTB mass extinction (Fig. 5A). This indicates that the early evolution of Danian species in P0 and lower part of P1a(1) is missing due to erosion or non-deposition (Fig. 4). About 30-cm above this hiatus subzone P1a(1) ends with another sudden faunal assemblage change marked by dramatically decreased *Guembelitria*, *P. eugubina* and

Please cite this article as: Punekar, J., et al., A multi-proxy approach to decode the end-Cretaceous mass extinction, Palaeogeogr. Palaeoclimatol. Palaeoecol. (2015), http://dx.doi.org/10.1016/j.palaeo.2015.08.025

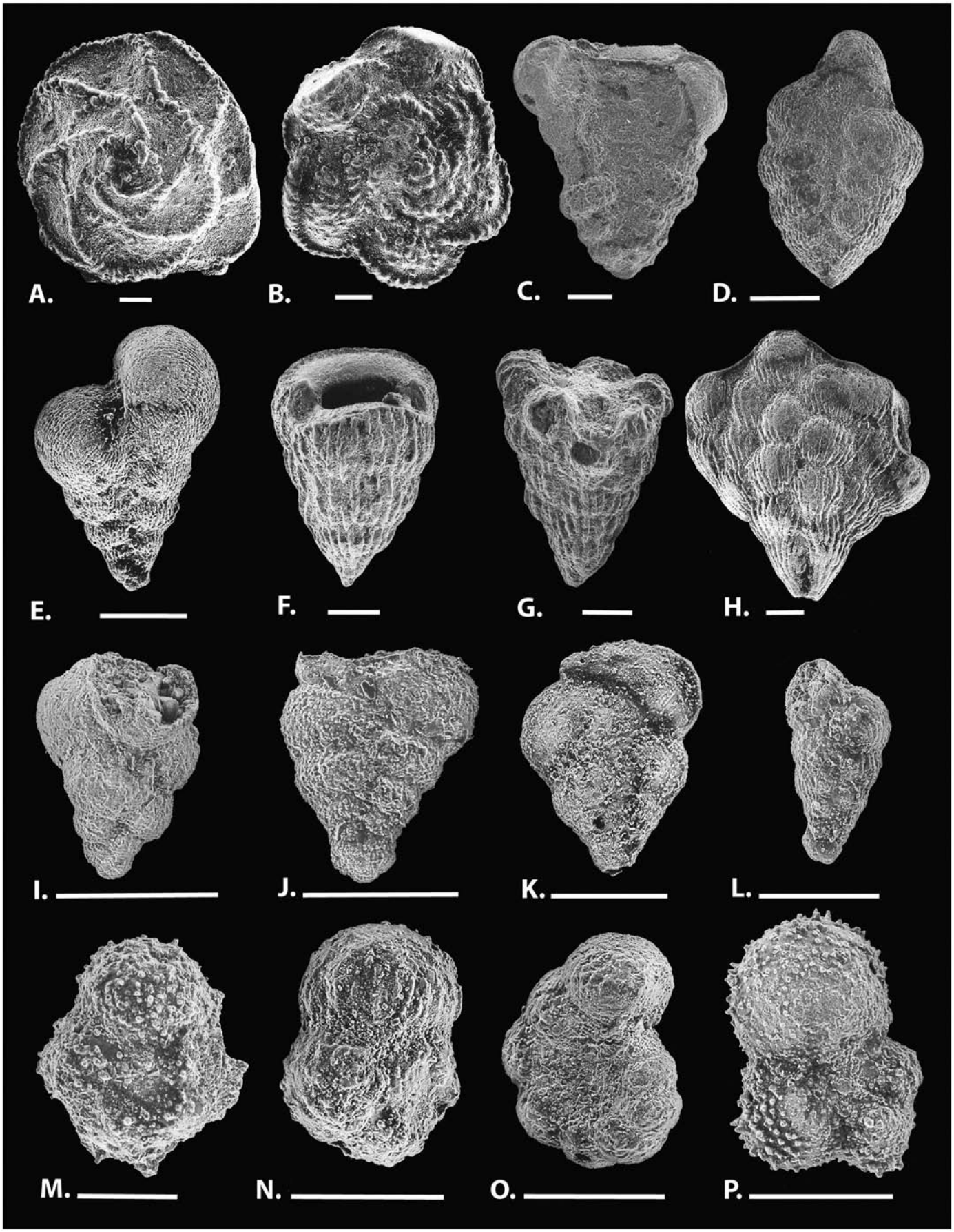

Please cite this article as: Punekar, J., et al., A multi-proxy approach to decode the end-Cretaceous mass extinction, Palaeogeogr. Palaeoclimatol. Palaeoecol. (2015), http://dx.doi.org/10.1016/j.palaeo.2015.08.025

P. longiapertura, a sudden appearance of abundant *Chiloguembelina morsei* and the FO of *S. triloculinoides* (Fig. 5A). This assemblage is indicative of subzone P1a(2) and marks another short hiatus between subzones P1a(1) and P1a(2) (Fig. 4). Hiatuses at the KTB and lower Danian (resulting from condensed sedimentation and/or deep-sea currents) have been documented worldwide in various studies (reviews in MacLeod and Keller, 1991; Keller et al., 2003, 2013).

At Gamsbach an early Danian hiatus is also present as evident by the diverse (12 species) early Danian assemblage including *P. pseudobulloides*, the index species for subzone P1a(2) directly overlying the mass extinction horizon (Fig. 6A). This indicates erosion of P0, P1a(1) and at least part of P1a(2) (Fig. 4). Another abrupt faunal change and hiatus occurs at the P1a(2)/P1b boundary about 30-cm above the KTB marked by the extinction of *P. eugubina* and *P. longiapertura* (index for top P1a(2)) and terminal abundance decrease in *Globigerina edita*. Above this hiatus abundant *C. morsei* and common *P. pseudobulloides* followed by abundant *Guembelitria* spp. indicates zone P1b (Figs. 4, 6A).

6. Stable isotpes and faual turnover

6.1. Stable isotopes

Whole-rock stable carbon and oxygen isotope data for Gamsbach (Austria) were obtained for this study (supplementary materials Table 7). Planktic, benthic and bulk stable isotope data for Elles (Tunisia) and whole-rock isotope data for Bidart (France) have already been documented (Stüben et al., 2003; Thibault and Husson, in press; Font et al., 2014). Visual inspection of preservation and degree of recrystallization of individual foraminifera tests indicated that the Gamsbach isotope data were likely to be the most compromised.

At Elles, the overall low $\delta^{18}O$ values (−7.0 to −4.0‰) for planktic as well as benthic (−4.5 to −2.0‰) foraminifera indicate diagenetic effects but long term trends may still be preserved (Stüben et al., 2003; supplementary materials Table 5). At Bidart, the whole-rock $\delta^{13}C$ values range between −1.7 and 1.8‰ and bulk $\delta^{18}O$ values range between −3.2 and −0.3‰. Plotting $\delta^{13}C$ vs. $\delta^{18}O$ values yields a correlation coefficient $R^2 = 0.53$, suggesting that diagenetic alteration of the primary signal may not be ruled out (supplementary materials Table 6). A low $\delta^{13}C$ event is recognized between 3.5 m and 0.75 m below the KTB. A similar event is also observed in the planktic $\delta^{13}C$ values at Elles between 1.75 m and 6.6 m below the KTB boundary indicating that this signal may be real (Fig. 7). A long term increasing trend through zone CF1 is observed in $\delta^{18}O$ profiles of Bidart, Gamsbach and Elles, although the values at Gamsbach and Elles record frequent fluctuations (Fig. 8). The whole-rock $\delta^{13}C$ values for Gamsbach range between 1.41 to 2.42‰ and the bulk $\delta^{18}O$ range between −2.6 and −1.1‰. The $\delta^{13}C$ vs. $\delta^{18}O$ correlation coefficient is lower than that for Bidart ($R^2 = 0.27$) but the poorly preserved fragmented and recrystallized tests suggest considerable overprint on the primary isotopic composition. The low $\delta^{13}C$ event of Bidart and Elles is not preserved at Gamsbach.

6.2. Faunal turnover

6.2.1. Bidart (France)

Maastrichtian planktic foraminifera at Bidart are recrystallized but relatively well preserved and identification is fairly easy. About 51 species were identified in the 63–150 μm size fraction and 23 species in the >150 μm size fraction (Fig. 5A). The species richness in the 63–150 μm fraction gradually drops from 30 to 20 through the analyzed interval of zone CF1. A rapid decline from ~20 species to 3 species is seen 3-cm below the KTB. A brief increase to 13 species occurs 2-cm above the boundary clay is observed in the small and large size fractions and is likely due to erosion and redeposition (Fig. 5A). In the >150 μm fraction, diversity remains nearly constant through CF1 but declines from ~50 species to 11 species at 3-cm below the KTB.

All typical late Maastrichtian globotruncanids, rugoglobigerinids, heterohelicids and pseudoguembelinids are represented, although the biserial heterohelicids and pseudoguembelinids dominate the assemblages in the 63–150 μm (Fig. 5B). In addition to common cosmopolitan species, biserial species *Hartella harti* and *Spiroplecta americana* Ehrenberg are also frequent in the assemblage (Plate 1: K, J); these species were first described by Georgescu and Abramovich (2009) from upper Maastrichtian sediments of the Atlantic Ocean. At Bidart *H. harti* and *Heterohelix navarroensis* are the most abundant and together constitute 40–60% of the assemblage throughout CF1 (Figs. 5B, 7; Plate 1: K, L). *Guembelitria* sp. is present in the 63–150 μm size fraction but not in the abundance observed in shallow marine KTB transitions (e.g. Egypt, Sinai, Tunisia (Seldja); Keller and Benjamini, 1991; Keller et al., 1997; Keller, 2003, 2004; Punekar et al., 2014b; Plate 1: I). The newly evolved Danian assemblage in zone P1a(1) is dominated by *Guembelitria sp.* and *Parvularugoglobigerina sp.* (30–40%, Fig. 5A). The P1a(2) assemblage is dominated by *Chiloguembelina midwayensis*. (see supplementary material Fig. S1 for planktic foraminifera in the >150 μm size fraction at Bidart).

6.2.2. Gamsbach (Austria)

A planktic foraminiferal study by Korchagin in Grachev et al. (2005) identified only 25 Maastrichtian species and placed this assemblage in the *Abathomphalus mayaroensis* zone, which spans most of the late Maastrichtian (68.72–65.5 Ma). The preservation of Maastrichtian planktic foraminifera in the 63–150 μm fraction at Gamsbach is very poor. Recrystallization and the difficulty of freeing specimens from surrounding sediments result in specimens with a highly fragmented and abraded appearance and no reliable quantitative data can be obtained for the Maastrichtian (supplementary material Fig. S2). In the >150 μm fraction preservation is better and therefore was analyzed quantitatively (Fig. 6B). A total of 46 species were identified in the >63 μm size fraction which is likely an underestimate of the total assemblage due to poor preservation. Most species are consistently present in the lower 1.25 m of the section. But in the uppermost 0.5 m, species are more sporadic and species richness drops from 46 to 21–30 species. In the >150 μm fraction, species richness ranges between 30–40 species and drops from ~25 to 8 species at the KTB (Fig. 6A).

All common Maastrichtian groups such as the globotruncanids, rugoglobigerinids, heterohelicids and pseudoguembelinids are present in the assemblage. *Pseudotextularia elegans*, *Pseudotextularia nuttali*, *Pseudoguembelina hariaensis*, *Heterohelix globulosa* and *Planoglobulina brazoensis* dominate the >150 μm fraction (Fig. 6B). *Guembelitria* sp. is almost absent in the 63–150 μm fraction. In contrast to Bidart, *H. harti* and *S. americana* are not present in the assemblage (Fig. 8C). In the Danian, the diversity in zone P1a(2) is about 10 species which increases to ~20 species in zone P1c. The P1a(2) assemblage overlying the KTB is dominated by *G. cretacea*, *P. eugubina*, *P. longiapertura*, *Globigerina edita*, *Globanomalina archaeocompressa* and *Praemurica taurica* (Fig. 6A).

6.3. Depth-ranked species

Planktic foraminifera species have been classified into surface dwelling opportunistic species *Guembelitria*, surface–subsurface mixed layer, intermediate or thermocline and deep-water dwellers based on stable oxygen and carbon isotope ranking of well-preserved specimens

Plate 1. Characteristic taxa of the upper Maastrichtian zone CF1 assemblage at Bidart, France, scale bar = 100 μm.A. *Globotruncanita stuarti* (de Lapparent), spiral view.B. *Abathomphalus mayaroensis* (Brönnimann), spiral view.C. *Heterohelix rajagopalani* Govindan.D. *Pseudoguembelina hariaensis* Nederbragt.E. *Heterohelix globulosa* (Ehrenberg).F. *Pseudotextularia elegans* (Rzehak).G. *Racemiguembelina fructicosa* (Egger).H. *Planoglobulina brazoensis* (Martin).I. *Guembelitria cretacea* (Cushman).J. *Spiroplecta americana* (Ehrenberg).K. *Hartella harti* Georgescu & Abramovich.L. *Heterohelix navarroensis* (Loeblich).M. *Plummerita* aff. *hantkeninoides* (Brönnimann).N. *Rugoglobigerina macrocephala* (Brönnimann).O. *Globigerinelloides volutus* (White).P. *Globigerinelloides subcarinatus* (Brönnimann).

Please cite this article as: Punekar, J., et al., A multi-proxy approach to decode the end-Cretaceous mass extinction, Palaeogeogr. Palaeoclimatol. Palaeoecol. (2015), http://dx.doi.org/10.1016/j.palaeo.2015.08.025

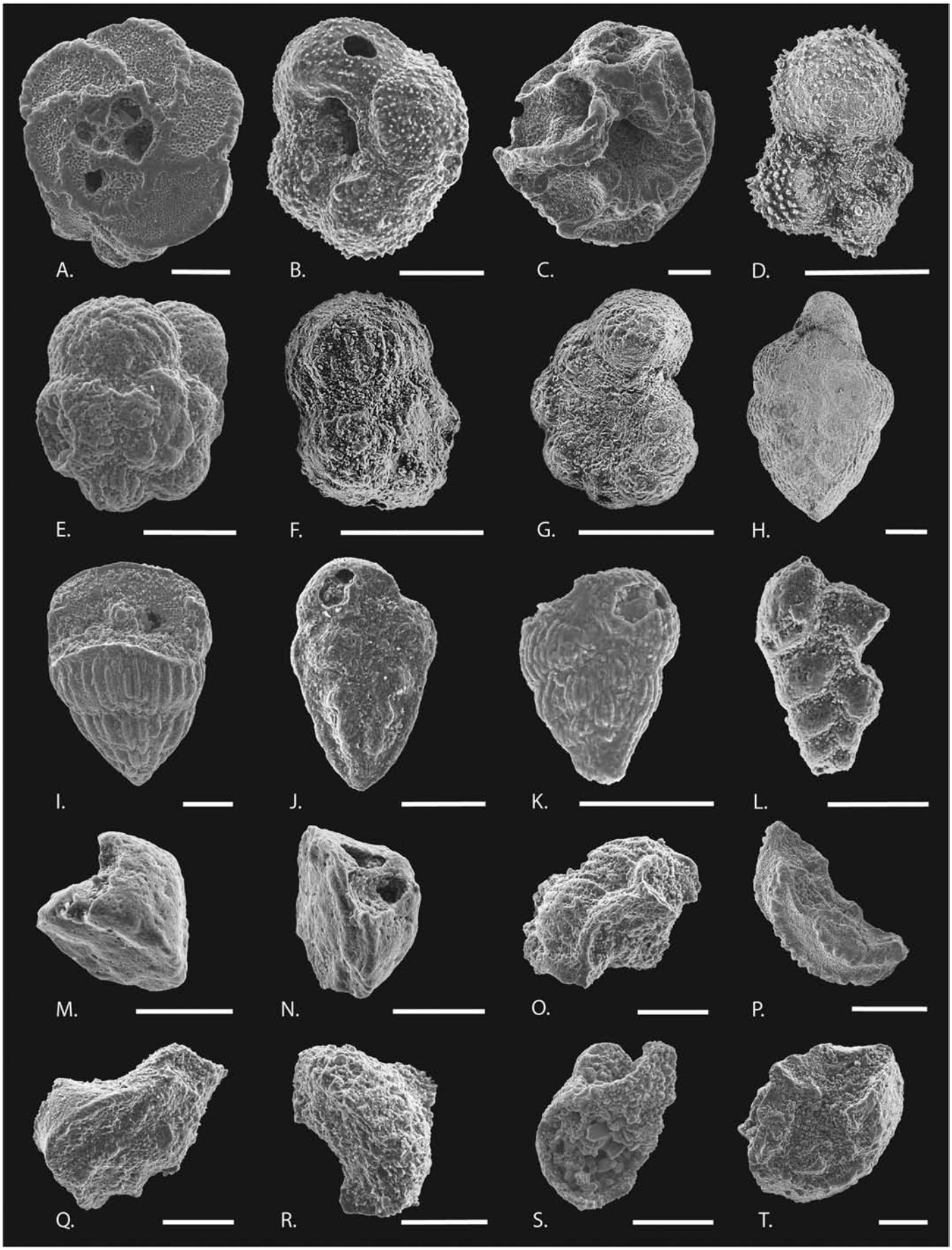

Please cite this article as: Punekar, J., et al., A multi-proxy approach to decode the end-Cretaceous mass extinction, Palaeogeogr. Palaeoclimatol. Palaeoecol. (2015), http://dx.doi.org/10.1016/j.palaeo.2015.08.025

(Abramovich et al., 2003, 2010). The diversity and abundance changes for each depth group can indicate climatic and environmental effects at different depths of the water column. Fig. 9 shows the diversity and abundance of the four groups in small (63–150 μm) and larger (>150 μm) size fractions analyzed through zone CF1 at Bidart and Gamsbach and compared with Elles, Tunisia (Supplementary material Section 5, Table 1 show the depth-ranked grouping of species used for this study).

At Bidart, the small sized opportunistic *Guembelitria* (63–150 μm fraction) are rare in the lower part of the section and slightly increase in the upper ~1.5 m below the KTB (Fig. 9B). This group is not as rare in Elles but the relative abundance is <10% (Fig. 9A). The subsurface mixed layer dwellers (Table 1) constitute 80–90% of the CF1 assemblage at both Bidart and Elles. In the small size fraction, this group at Bidart with 30–40 species is almost twice as diverse as at Elles, (10–20 species). In the >150 μm fraction, the relative abundance of mixed layer dwellers constitute 60–80% at Bidart and ~80% at Elles (Fig. 9A, B). Their diversity fluctuates through CF1 and shows a gradual decrease from ~20 to 14 species followed by a rapid decline ~3 cm below the KTB. The thermocline dwelling globotruncanids are rare in the small size fraction at both Bidart and Elles with relative abundance <5%. Two peaks of increased abundance and diversity are noted in the upper 30-cm of late Maastrichtian at Bidart and in the last meter at Elles. In the >150 μm fraction, thermocline dwellers are more abundant (20–30%) at Bidart compared to the same group in Elles (<10%). The sub-thermocline deep-water dwellers in both size fractions at Bidart and Elles show consistently low abundances (<5%) and diversity (<3 species) throughout zone CF1 (Fig. 9A, B).

At Gamsbach the mixed dwellers dominate in the larger size fraction, with ~70% relative abundance, followed by the thermocline dwellers with 25–30% abundance. The high abundance of thermocline dwelling globotruncanids in Gamsbach is more comparable to the assemblage at Bidart than that at Elles (Fig. 9C). The deep dwellers are represented by 1–3 species and account for <10% throughout CF1.

The faunal assemblage differences between Elles vs. Bidart and Gamsbach appear to be related to deposition in a relatively shallow continental shelf vs. deep middle bathyal environments. This is indicated by the similarity in the faunal compositions between Bidart, Gamsbach and the middle bathyal DSDP Site 525A, but dissimilarity with Elles. For example (1) there is significantly higher relative abundance of *P. hariaensis* at Bidart (20–25%), Gamsbach (10–20%) and Site 525A (10–20%), compared with Elles (<5%) Abramovich and Keller, 2002, 2003); (2) *Heterohelix globulosa* is less abundant in the >150 μm fraction at Bidart (15–20%), Gamsbach (<10% with acme of 20%) than at Elles (40–50%); (3) *Planoglobulina brazoensis* is more abundant (5–10%) in all three deeper sections, but rare at Elles; and (4) *Globotruncana arca* is more abundant at Bidart (10%), Gamsbach (10–20%) and Site 525A (20–30%) than at Elles (<5%).

7. Dissolution-based proxies for ocean acidification

7.1. Magnetic susceptibility (MS)

Magnetic susceptibility (MS) of marine deposits depends essentially on their mineralogical composition, and includes contributions (in proportion to their abundance) from all – diamagnetic (e.g., calcite), paramagnetic (e.g., clay) and ferromagnetic (ex: magnetite) – minerals present in the sediment. Since the pristine signal of magnetic susceptibility in marine sediment reflects the balance between detrital input (high MS) and carbonate productivity (low MS), it represents a robust paleoenvironmental indicator.

The rock magnetic properties for Elles are published in Stüben et al. (2003) and for Bidart in Font et al. (2011, 2014) and Font and Abrajevitch (2014).

Mass specific magnetic susceptibility values of the Maastrichtian marls from Elles are in the range of 10^{-7} to 10^{-6} m^3/kg, and comparable to other marine sediments worldwide (Ellwood et al., 2008). The overall MS profile for zones CF3–CF1 shows a positive correlation with percent phyllosilicates and an inverse correlation with carbonate content, indicating a strong relationship between MS, climate (precipitation and runoff) and/or sea-level rise. The KTB is featured by an abrupt shift in MS values, probably resulting from an abrupt change in lithofacies (i.e. the clay layer). The Elles section does not show the typical low MS interval below the KT boundary as in Bidart (Fig. 10A). At Bidart the average MS value is 1.85×10^{-7} m^3/kg for the lower part of zone CF1 and ~0.84×10^{-7} m^3/kg for the final ~60 cm that forms the benchmark interval. The characteristic abrupt increase in MS values (to 4.62×10^{-7} m^3/kg, likely due to or a very rapid change in sedimentation) marks the KTB hiatus at Bidart (Fig. 10B). For the Gambsach section, the mass specific magnetic susceptibility of 49 samples excluding turbiditic levels was measured (Fig. 10C). Maastrichtian MS values range between 10^{-8} to 10^{-7} m^3/kg. The average MS value for the lower part of zone CF1 is $6.7 \times 10^{-8}$$m^3$/kg. About ~60 cm below the KTB, MS values reach a minimum of $4.5 \times 10^{-8}$$m^3$/kg (average of $5.1 \times 10^{-8}$$m^3$/kg). These low MS values persist over an interval of 36-cm. Across the KTB MS values show the typical increase culminating at $2.3 \times 10^{-7}$$m^3$/kg, similar to Bidart and other KTB sections (e.g., Gubbio, Oman: Ellwood et al., 2003; Atlantic ODP 1259: Erbacher et al., 2004; North Atlantic ODP 1049A: Moore et al., 1998).

7.2. Percent calcium carbonate

Whole-rock percent $CaCO_3$ content of marine sediments is the net result of the local paleaoclimate, calcareous nannoplankton and calcareous dinoflagellate palaeoproductivity, planktic foraminiferal abundance, water column pH/dissolution, pore-water dissolution/recrystallization and detrital influx. For localities with greater terrigenous influx the ratio of Ca/detritus is a better estimate of biogenic $CaCO_3$ as it accounts for the detrital contribution. At Elles, the calcite/detritus ratio is low (0.5) near the base of zone CF1 (8–10 m below the KTB, Fig. 10A). In this interval, the phyllosilicate content is relatively high (25–35%) with an increasing trend. The Ca/detritus ratio fluctuates but increases to 0.75–1.00 about 5–8 m below the KTB along with an increase in MS values. The Ca/detritus ratio is higher in the top 4 m of zone CF1, albeit with three sharp decreases.

The percent $CaCO_3$ at Bidart gradually decreases from 55% at the base of zone CF1 to about 40% 2 m below the KTB. An increase to 50% is observed 1.5 m below KTB followed by values between 40–50% up to the low MS interval where values sharply increase to 60% about 0.25 m below the KTB (Fig. 10B). At Gamsbach, $CaCO_3$ ranges between 40–50% and records several abrupt decreases in zone CF1 correlative with abrupt changes in percent quartz and MS values (Fig. 10C). In the 1 m below the KTB $CaCO_3$ varies between 55–80% with the largest drop ~20 cm below the KTB correlative with increased phyllosilicates and MS values. A drop in $CaCO_3$ to nearly zero percent is indicated in the KTB clay in all three sections.

7.3. Fragmentation index

Tests of planktic as well as benthic foraminifera may undergo fragmentation due to a multitude of taphonomic processes. Acidic ambient waters react with planktic foraminiferal test carbonate, which leads to test dissolution and enhanced fragmentation. The number of fragments

Plate 2. Planktic foraminifera indicating varying degrees of preservation in the upper Maastrichtian zone CF1 assemblage at Bidart, France, scale bar = 100 μm.(A–L): "Imperfect" tests with minor breakages and/or holes and signs test surface dissolution.(M–S): "Fragments" defined by less than two-thirds or the original test preserved.

Please cite this article as: Punekar, J., et al., A multi-proxy approach to decode the end-Cretaceous mass extinction, Palaeogeogr. Palaeoclimatol. Palaeoecol. (2015), http://dx.doi.org/10.1016/j.palaeo.2015.08.025

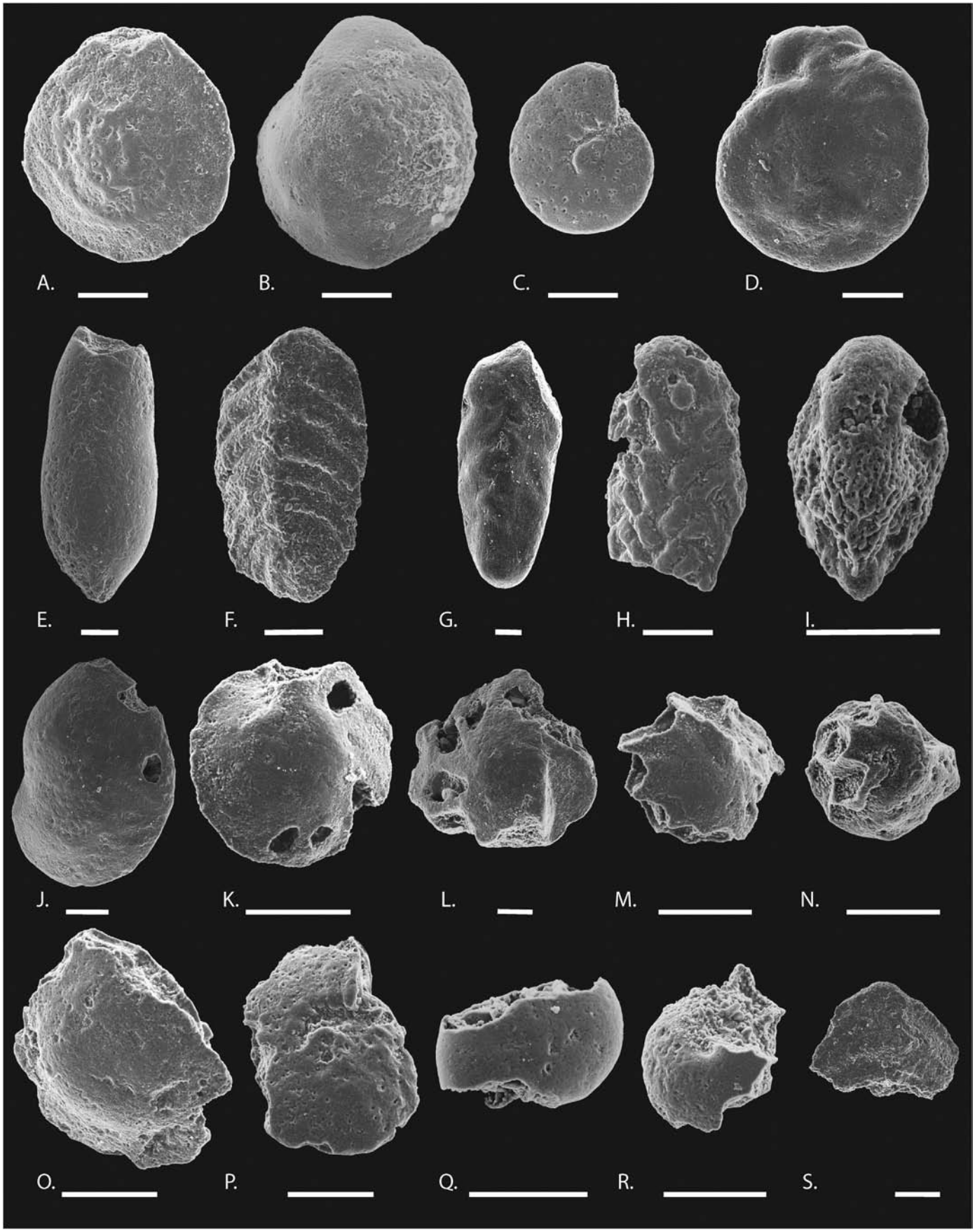

Plate 3. Benthic foraminifera indicating varying degrees of preservation in the upper Maastrichtian zone CF1 and the KTB assemblage at Bidart, France, scale bar = 100 μm. (A–G): "Perfect" tests with no signs of chemical or mechanical damage. (H–L, O, P): "Imperfect" tests with minor breakages and/or holes and signs test surface dissolution. Note that the proportion of the tests with holes is maximum at the KTB and in the early Danian sediments. (M, N, Q–S): "Fragments" defined by less than two-thirds or the original test preserved.

Please cite this article as: Punekar, J., et al., A multi-proxy approach to decode the end-Cretaceous mass extinction, Palaeogeogr. Palaeoclimatol. Palaeoecol. (2015), http://dx.doi.org/10.1016/j.palaeo.2015.08.025

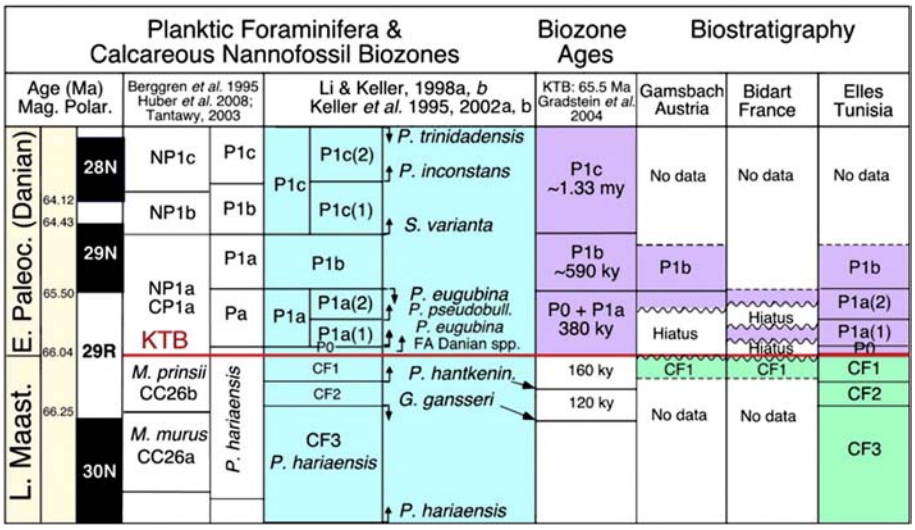

Fig. 4. The completeness of Bidart and Gamsbach sections relative to Elles (Tunisia) based on planktic foraminiferal biozonation scheme of Keller et al. (1995), Li and Keller, (1998a,b) and Keller et al. (2002a,b). The biozone ages can be extrapolated using a KTB age of 65.5 Ma (Gradstein et al., 2004) or 66.04 Ma (Renne et al., 2013). Hiatuses are observed at the KTB and at the P1a(1)/P1a(2) transition at Bidart. A major hiatus is identified at the KTB at Gamsbach due to missing zones P0, P1a(1) and early P1a(2).

have been used as a quantitative estimate of low pH in foraminiferal assemblages (Thunell, 1976; Berger et al., 1982). The fragmentation index may be calculated based on the following equation (Williams et al., 1985; Malmgren, 1987):

$$\text{Fragment } \% = (\text{Fragments}/8)/[(\text{Fragments}/8) + \text{whole tests}]$$

Based on the assumption that each (non-crystallized) test breaks into an average of 8 fragments, the equation requires the total number of counted fragments to be divided by 8 to estimate the original number of whole tests. This is because the number of fragmented tests is a better approximation of dissolution effects than the total number of fragments counted (Le and Shackleton, 1992). As most of the planktic foraminifera at Bidart, Elles and Gamsbach are recrystallized and/or infilled with secondary calcite, they are relatively more resistant to fragmentation than pristine tests. We adjust for recrystallization by reducing the number of fragments per test to 6 instead of 8 to avoid underestimation of fragmented tests. Similarly, we consider 2 fragments per test for benthic foraminifera for Bidart as they are far more resistant to fragmentation.

The stacked area graphs of Fig. 10 show fragmentation indices for Elles, Bidart and Gamsbach. At Elles, fragmented tests increase from 23% to 46% at the beginning of the low MS interval and increased fragmentation and imperfect tests are observed in the top 4 m below the KTB (Fig. 10A). At Bidart, the percentage of imperfect tests for the lower part of CF1 is considerably higher than at Elles and that of fragmented tests is lower (Fig. 10 A–B). In the uppermost ~60 cm of zone CF1, the low-MS interval is accompanied by a significant ($p < 0.0001$) increase in the combined abundance of imperfect and fragmented from ~25% to 70% (~0.3 m below KTB, Fig. 10B). A drop in this percentage ~2.5 m below the KTB boundary is followed by a rapid increase to 90%. It must be noted that the fragmented tests (not the imperfect tests) dominate at the KTB boundary hiatus. The fragmentation index at Gamsbach also shows an abrupt increase in the combined abundance of fragmented and imperfect tests from 40% to ~90% at the onset of the low MS interval ~50 cm below the KTB boundary. Within this interval, fragmentation continues to be high (~90%) up to the KTB boundary (Fig. 10C). A brief episode of decreased fragmentation is observed ~20 cm below the KTB boundary similar to the event recorded at Bidart (supplementary material Tables 2–4). Fig. 11 compares the fragmentation indices of planktic and calcareous benthic foraminifera at Bidart. The proportion of fragments of benthic foraminifera remains 2–3% for most of the analyzed CF1 interval (Plate 3: M, N, Q–S). This is consistent with the general robustness of benthic morphologies and likely indicates a limited/uniform influence of sample processing techniques and post-depositional breakage on the assemblage. However, an increase in the fragments to ~5% concurrent with the Deccan benchmark event may imply enhanced post-depositional bottom water transport during the climate-cooling event (Figs. 10, 11). The imperfect benthic tests of CF1 largely show mechanical damage unlike the planktic counterparts that show chemically leached surfaces and holes (Plate 2: A–L). However, at the KTB and the lowermost Danian, sediments contain benthic foraminifera that show intense leaching as well as mechanical damage strongly indicating a dominance of post-depositional dissolution and bottom water transport affecting the assemblage. The planktic FI is not useful to isolate water column dissolution effects in these samples (Fig. 11).

7.4. Preferential preservation of robust morphologies

Dissolution preferentially decreases the relative abundance of thin-walled test morphologies and therefore increases the relative abundance of robust dissolution-resistant tests (e.g. *Globotruncana*, *Globotruncanita*, *Pseudotextularia* and *P. brazoensis*), which may explain the increased calcite at this interval. This bias is evident just below the KTB mass extinction in all three profiles analyzed. In the middle shelf environment of Elles, globotruncanids and pseudotextularids are rare in zone CF1 (~1%), increase to 2% in the low-MS interval and peaks at 10% and 6% in the 1 m preceding the mass extinction (Fig. 10A). In the middle bathyal sections of Bidart and Gamsach, the abundance of globotruncanids average 20–30% throughout zone CF1. At Bidart globotruncanids abruptly reach 70% correlative with increased fragmentation and decreased percent $CaCO_3$ beginning about 30-cm below the KTB (Fig. 10B). At Gamsbach, globotruncanids and another robust species (*Planoglobulina brazoensis* show anomalously high abundance throughout zone CF1 with peak abundance of *P. brazoensis* correlative with the high fragmentation index ~15 cm below the KTB (Fig. 10C).

8. Discussion

8.1. Paleoclimate

Whole-rock stable oxygen and carbon isotopes approximate mixed layer (mostly calcareous nannoplankton) values in the deep-water

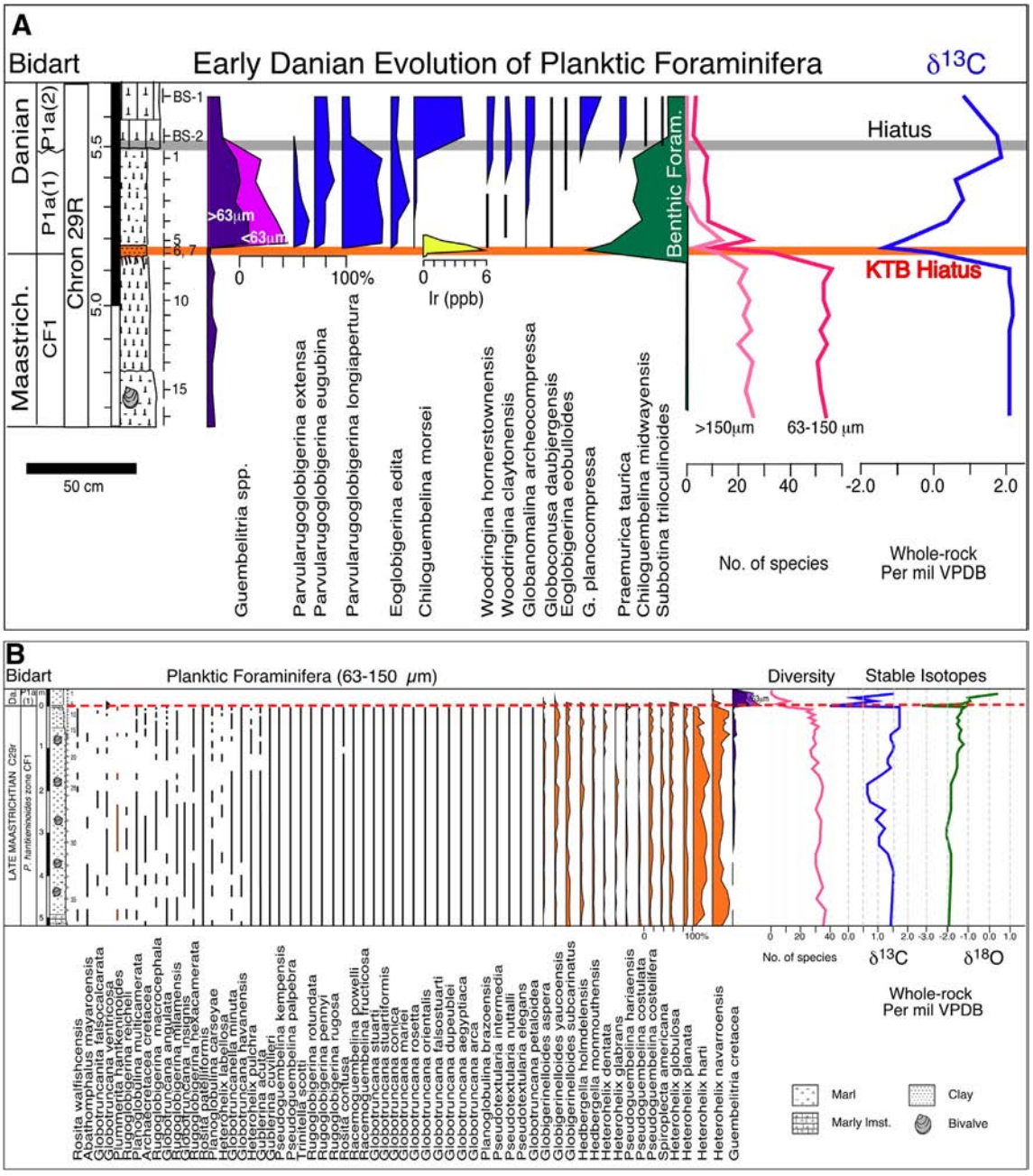

Fig. 5. (A) Key foraminifera and geochemical attributes of the KTB boundary and lower Danian at Bidart (B) Abundance of late Maastrichtian planktic foraminifera of the 63–150 μm size fraction and the KTB mass extinction. The $\delta^{13}C$ record shows the characteristic ~2‰ negative shift at the KTB.

sediments at Bidart and Gamsbach. Diagenesis and recrystallization of tests may have overprinted $\delta^{18}O$ signals but their effects on the $\delta^{13}C$ trend are limited. This claim is supported by the low correlation coefficients of $\delta^{13}C$ vs. $\delta^{18}O$ (Stüben et al., 2003; $R^2 = 0.53$ for Bidart and $R^2 = 0.27$ for Gamsbach) and the low correlation coefficient of $\delta^{13}C$ v/s $\%CaCO_3$ ($R^2 = 0.40$ for Bidart and $R^2 = 0.39$ for Gamsbach).

The lower ~3 m of zone CF1 at Bidart and lower ~1.2 m of Gamsbach record faunal responses comparable with those observed in the upper part of the late Maastrichtian global warming at Elles and DSDP Site 525A. Globally, this warm event began in zone CF2 as a likely consequence of the onset of the main phase-2 of Deccan volcanism (Punekar et al., 2014a). This is consistent with the more negative $\delta^{18}O$ values for these intervals indicating higher temperatures (−2‰ for Bidart and −1.5 to −2‰ for Gamsbach, Fig. 8). At Bidart, the late Maastrichtian warm event is associated with changes in the relative abundance of heterohelicids (particularly *H. planata*, *H. navarroensis* and *H. globulosa*) and increased *P. hariaensis* abundance in the >150 μm fraction.

The end of the late Maastrichtian warming at Elles is marked by abrupt cooling concurrent with unprecedented low MS values and increased test fragmentation ~4 m below the KTB. This could be an expression of increased volcanic SO_2 emission and acidification (Fig. 10 this study; Fig. 5 of Stüben et al., 2003). At Bidart the onset of this same cooling event is recognized by a drop in MS associated with increased dissolution and disappearance of *Globigerinelloides yaucoensis*, *P. costulata*, *G. subcarinatus* and *R. rugosa* and at Gamsbach the disappearance of *G. subcarinatus* (Figs. 8, 10).

8.2. Paleoproductivity

Low $\delta^{13}C$ values with multiple negative excursions are observed at Elles and Bidart (~0.5‰ and ~0.7‰ respectively) near the end of

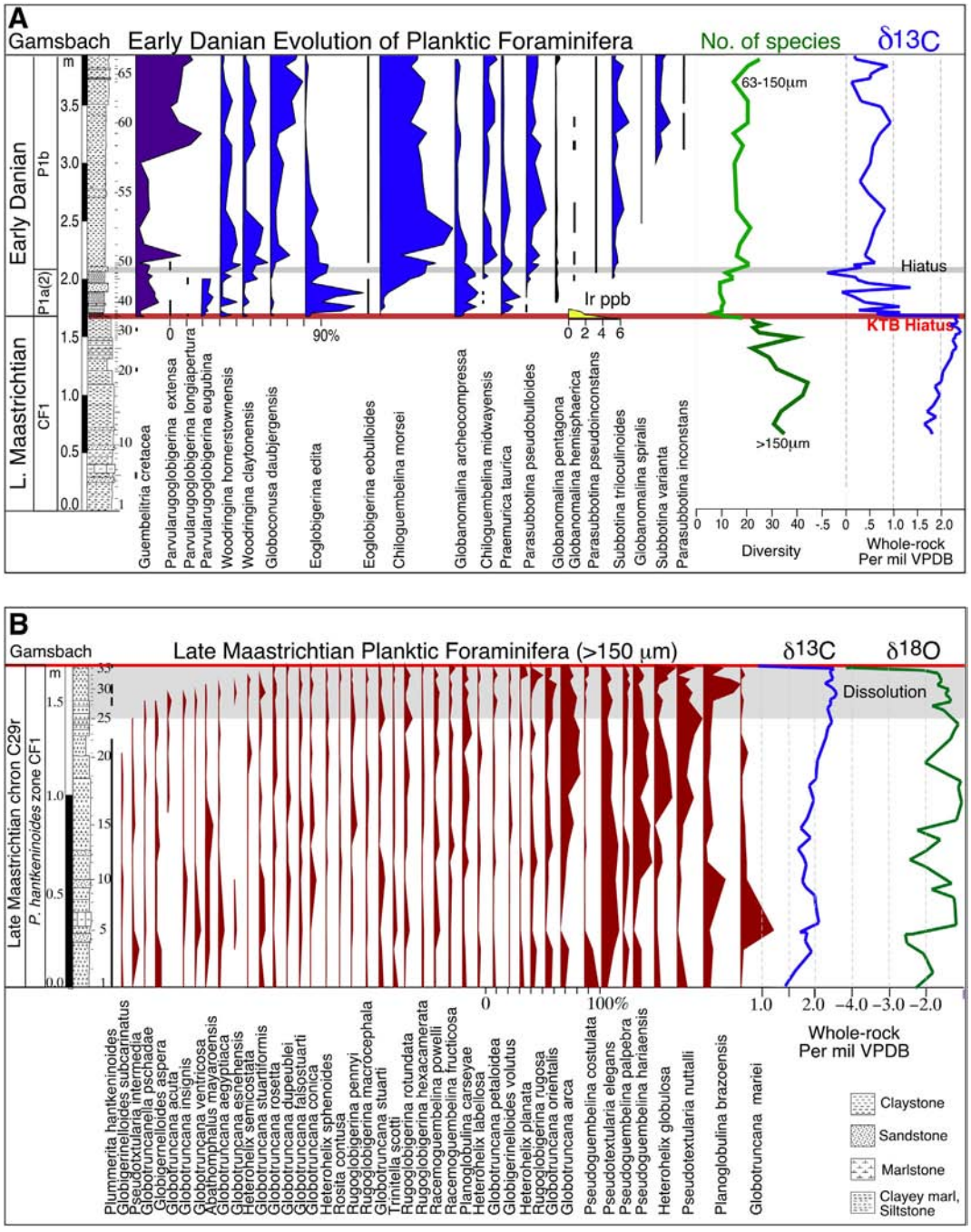

Fig. 6. (A) Faunal and geochemical changes at the KTB boundary and in the lower Danian of Gamsbach. (B) Late Maastrichtian planktic foraminifera of the >150 μm size fraction and the KTB mass extinction. The $\delta^{13}C$ record shows ~1.3‰ negative shift at the KTB.

the late Maastrichtian CF1 warm event Fig. 7). Similar negative excursions (~1‰) are recorded at deep marine Site 525A (~0.3‰) as well as in shallow marine environments of Texas and India (Meghalaya) (Li and Keller, 1998a; Abramovich et al., 2011; Gertsch et al., 2011). The existing dataset shows a greater magnitude of $\delta^{13}C$ negative shift in the shallow sites (e.g., Meghalaya (India), Mullinax-1 (Texas) and slightly deeper Elles (Tunisia). The smaller $\delta^{13}C$ shift at deeper Site 525A may be due to an incomplete record resulting from erosion of early Danian and topmost Maastrichtian sediments (Li and Keller, 1998a).

A rise in sea level near the end of the Maastrichtian and across the KTB transition accompanied by increased precipitation and continental weathering/erosion (Haq, 1988; Li et al., 1999) may have been responsible for the increased delivery of organic carbon with very low $\delta^{13}C$ values into shallow marine environments. Low primary productivity could have been the other important contributor to the low $\delta^{13}C$ values. Low nannofossil productivity is recorded in Elles, Bidart, DSDP Site 525A, DSDP Site 577A and DSDP Site 216 during the late Maastrichtian warm event in CF1 (Gorostidi and Lamolda, 1995; Gardin, 2002; Tantawy et al., 2009; Thibault and Gardin, 2007, 2010). Heterotrophic planktic foraminifera may have in turn suffered, resulting in a decrease in carbonate export and the eventual $\delta^{13}C$ value of bulk carbonate. The lower carbonate (40%) between 1.2–3.0 m below the KTB at Bidart, correlative with the low $\delta^{13}C$ interval lends support to this interpretation.

These global effects of increased precipitation and enhanced continental weathering/erosion can be attributed to climate warming caused by ongoing large scale Deccan volcanism. Additionally, the outgassing of higher-than-background quantities of volcanic CO_2 ($\delta^{13}C$ about −5‰)

Please cite this article as: Punekar, J., et al., A multi-proxy approach to decode the end-Cretaceous mass extinction, Palaeogeogr. Palaeoclimatol. Palaeoecol. (2015), http://dx.doi.org/10.1016/j.palaeo.2015.08.025

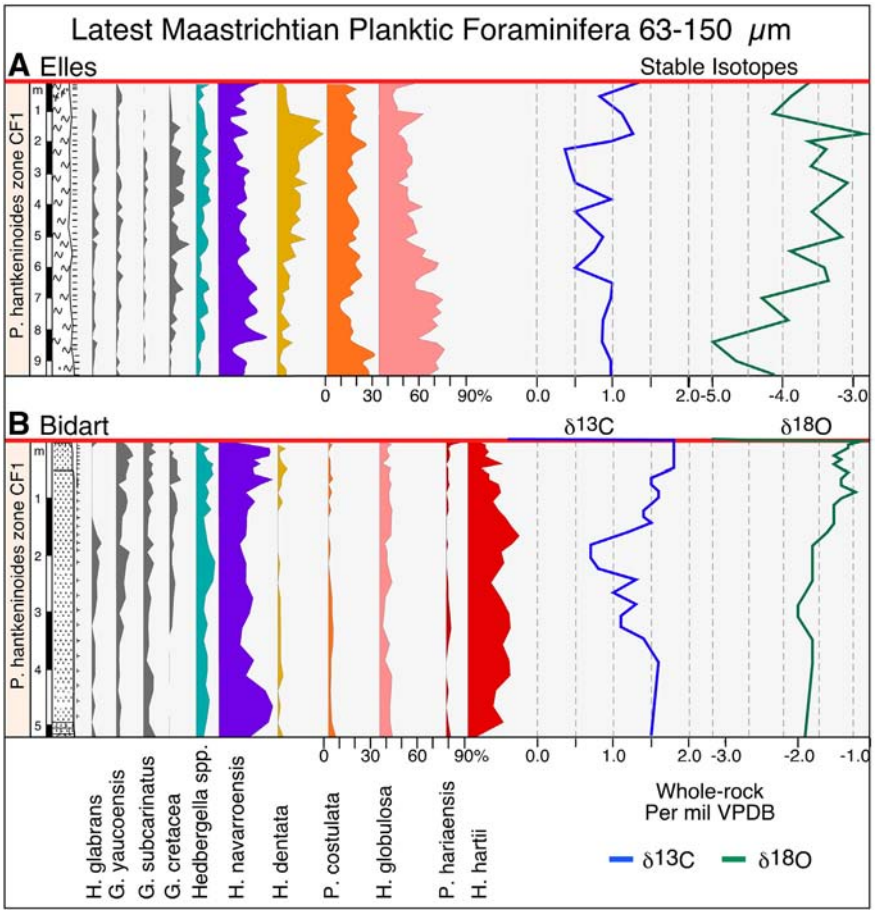

Fig. 7. A comparison of the relative abundances of some key species (63–150 μm) in the upper Maastrichtian zone CF1 assemblage of (A) Elles (Tunisia) and (B) Bidart (France). Note that *Heterohelix dentata*, *H. globulosa* and *Pseudoguembelina costulata* dominate the assemblage in Elles, in contrast to Bidart where they are rare. Whole-rock $\delta^{13}C$ and $\delta^{18}O$ are shown.

would also significantly contribute to lowering the $\delta^{13}C$ of the global oceans dissolved inorganic carbon (DIC), although the sediment record of this signal would lag by ~1000 years (Zeebe, 2012).

8.3. Planktic foraminifera

The high abundance of planktic and near absence of benthic foraminifera at Bidart is consistent with the high planktic:benthic ratio (>90% planktics) reported by Coccioni and Marsili (2007). The middle bathyal paleobathymetry and open marine setting appears to be the reason for the unusual globotruncanid abundance at Bidart and Gamsbach (Fig. 9). This is supported by the high abundance of globotruncanids at Site 525A (~35–40%, >150 μm) where deposition occurred at ~1000 m depth (Shackleton and Boersma, 1985; Abramovich and Keller, 2003). In relatively shallow (<150 m) continental shelf environments, such as Elles, the diversity and abundance of globotruncanids is much lower (Fig. 9).

8.4. Pre-KTB ocean acidification

White et al. (1994) showed that under present-day conditions (pH rain = 5.6), magnetite grains have very long time residence (>10^7 years) on land, but can be rapidly dissolved under more acidic conditions. In marine sediments, iron oxide dissolution by ocean acidification has previously been documented for the Triassic–Jurassic mass extinction and the coeval Central Atlantic Magmatic Province (Abrajevitch et al., 2013), and more recently in the case of the KTB mass extinction at Bidart and Gubbio (Font et al., 2014). The top ~50 cm interval of low-magnetic susceptibility (MS) that immediately precedes the KTB at Bidart was attributed to the main phase-2 of Deccan volcanism (Font et al., 2011, 2014; Font and Abrajevitch, 2014). The reductive iron oxide dissolution may have occurred on land and/or in seawater. The first scenario was tested by Font et al. (2014) who used a numerical weathering model to test for the consequences of acidic rains on a continental regolith. Results revealed nearly complete magnetite dissolution after ~31 kyr (with a pH of 3.3.). However, the dissolution of magnetotactic bacteria, which generally thrive the oxic–anoxic boundary in deep-sea marine sediments, evokes ocean acidification as well and requires validation (Font and Abrajevitch, 2014; Abrajevitch et al., 2015).

Factors affecting the nature and concentration of detrital magnetic minerals and therefore the MS of sediments include the nature and proximity of continental sediment sources carbonate productivity, sea-level changes and/or post-depositional alteration mechanisms (oxidation due to weathering/diagenetic reduction of oxides). The influence of sea level change on bulk MS is based on the relative contribution of carbonate (diamagnetic, low MS) versus detrital input (paramagnetic clays and ferromagnetic iron oxides, high MS) and thus can be estimated by correlating MS data with phyllosilicates where a direct positive correlation implies a strong dependence of both parameters.

At Elles, the pre-KTB low-MS interval is not evident probably because paramagnetic minerals (clays) dominate the MS signal, supported by very low Ca:detritus ratios (Fig. 10). At Bidart, the correlation between percent phyllosilicates and MS in zone CF1 is poor ($r = 0.088$), indicating an overall weaker influence due to sea level changes or turbidity currents. For Gamsbach, this correlation is more complicated due to the presence of frequent turbidite beds that are rich in dia/paramagnetic-silicates (Fig. 10; samples Gb 5, 10, 12, 15, 27–28). However, the MS profile of Gambsach does show low MS values for the ~40 cm interval below the KTB, similar to the MS profile of the Bidart section (Fig. 10). The MS data of the present study thus suggest that

Please cite this article as: Punekar, J., et al., A multi-proxy approach to decode the end-Cretaceous mass extinction, Palaeogeogr. Palaeoclimatol. Palaeoecol. (2015), http://dx.doi.org/10.1016/j.palaeo.2015.08.025

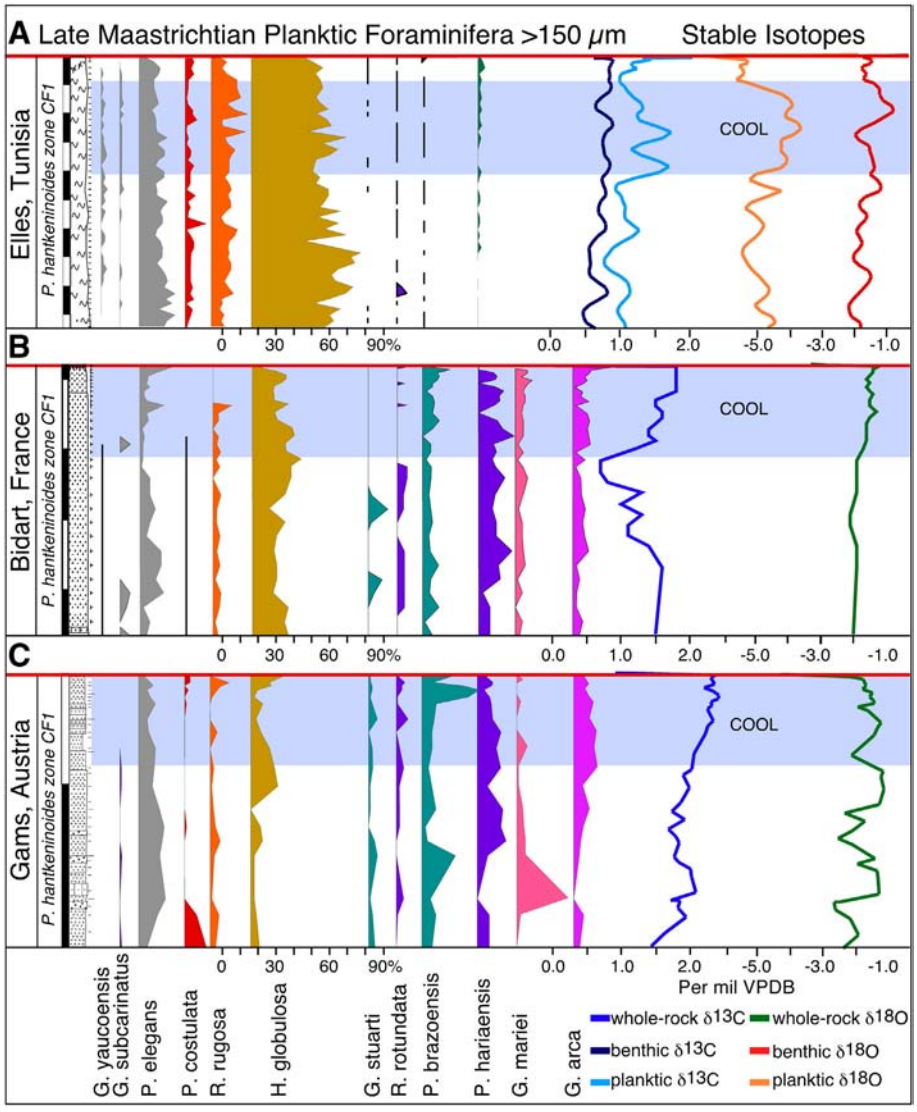

Fig. 8. A comparison of the relative abundances of some key species (>150 μm) in the Late Maastrichtian zone CF1 assemblage of (A) Elles (Tunisia), (B) Bidart (France) and (C) Gamsbach (Austria). The deep-water assemblages of Bidart and Gamsbach are very similar to each other and different from the neritic assemblages of Elles. Planktic $\delta^{13}C$ and $\delta^{18}O$ for Elles are obtained from *Rugoglobigerina rugosa* and benthic values are from *Cibicidoides pseudoacuta*. Whole-rock isotope data are shown for the Bidart and Gamsbach sections. (For interpretation of the references to color in this figure legend, the reader is referred to the web version of this article.)

the Gambsach section is a good analog of the Bidart section. A prolonged period of acid rain on the continents resulting in dissolution of magnetic detrital minerals can therefore be the principal mechanism that caused the low MS intervals antecedent to the KTB because sea level changes are a secondary influence on the MS profiles of Bidart and Gamsbach,

Surface ocean acidification in the low MS intervals of Bidart and Gamsbach is indicated by increased dissolution and fragmentation of planktic foraminiferal tests (Fig. 10). This increased fragmentation interval correlates with the abrupt cooling event at Elles (~4 m to ~0.5 m below the KTB), Bidart (~0.5 m interval below the KTB) and Gamsbach (~0.4 m interval below the KTB) despite their different paleogeography, paleobathymetry, depositional conditions and faunal assemblages, suggesting a common cause. An increase in the proportion of dissolved tests (in addition to physically fragmented ones) in Bidart and Gamsbach confirm the contribution of chemical leaching as cause for imperfect carbonate tests with holes. This implies that water column acidification is a likely cause for the observed increase in FI.

Benthic foraminifera are well preserved and even pristine looking in the same samples alongside leached and fragmented planktic foraminiferal tests at Bidart and Gamsbach (Plates 2, 3). This may indicate acidification restricted to the upper water column, or may reflect the inherently more robust mechanically resistant benthic tests. Alegret et al. (2004; Fig. 4) noted an increase in the proportion of agglutinated foraminifera relative to calcareous benthic foraminifera in the top 10-cm of the Maastrichtian at Bidart. We confirm these to be arenaceous (do not dissolve with 1:1 HCl), which may be interpreted as a consequence of ocean acidification or dissolution. Only in the KTB red clay layer are benthic species corroded suggesting that low pH acidic waters reached through the water column into deeper waters precisely at the KT boundary event. However, the benthic species were little affected by the KTB mass extinction or ocean acidification as their survival is globally documented (Widmark and Malmgren, 1992; Alegret et al., 2001, 2003. Alegret and Thomas, 2004). For the most part preceding the KTB, ocean acidification was restricted to the upper water column with surface waters in equilibrium with very high atmospheric pCO_2 and low CO_3^{2-} concentrations. Dissolution of test calcite during sinking through the water column would make tests more fragile in post-depositional transport. The degree of dissolution/fragmentation appears to be largely affected by local paleobathymetry and species composition of the assemblage.

At Elles, the percentage of fragments is high throughout zone CF1 owing to greater bottom water currents at shallower depths and also

Please cite this article as: Punekar, J., et al., A multi-proxy approach to decode the end-Cretaceous mass extinction, Palaeogeogr. Palaeoclimatol. Palaeoecol. (2015), http://dx.doi.org/10.1016/j.palaeo.2015.08.025

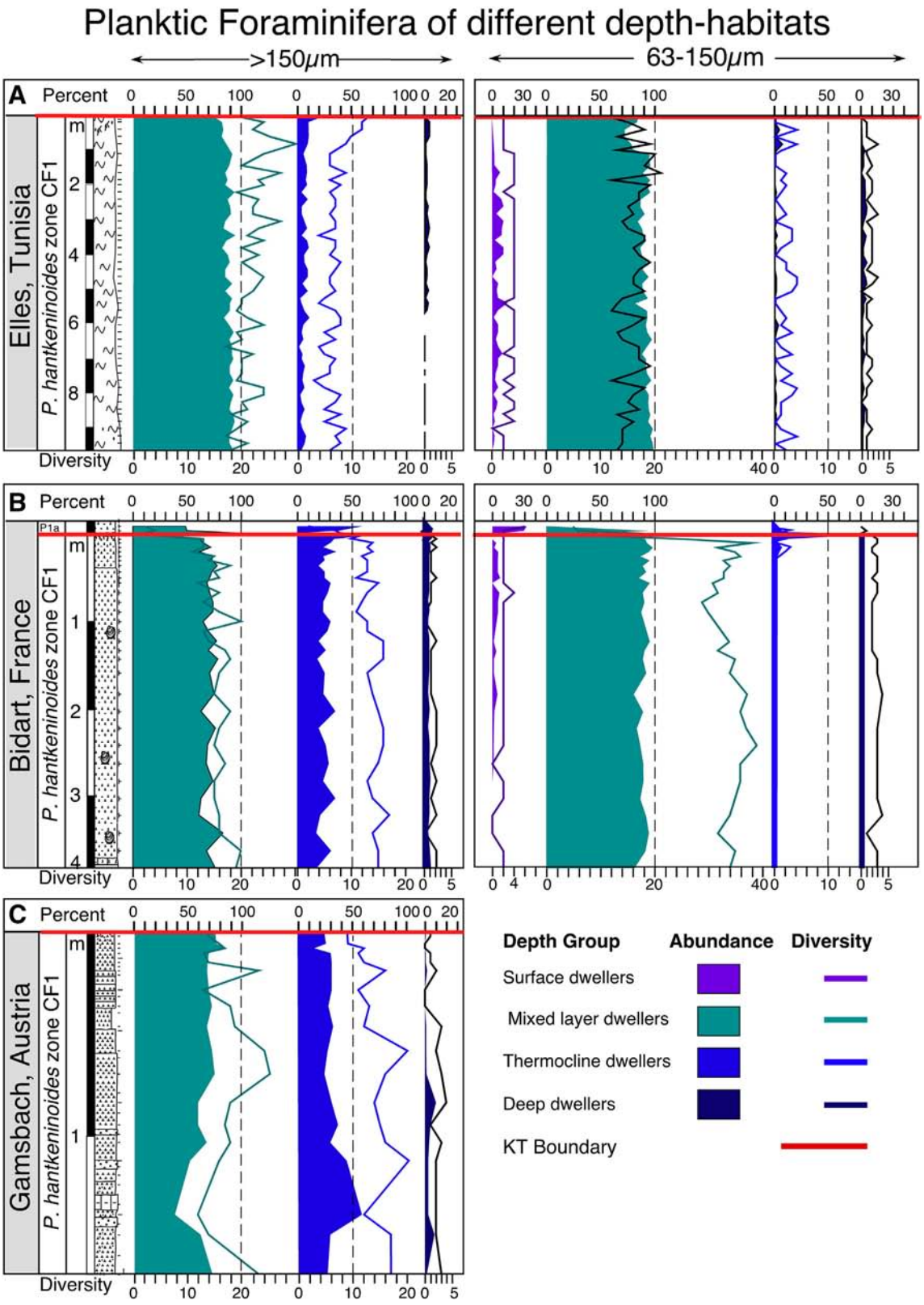

Fig. 9. Relative abundances of depth-ranked groups of planktic foraminifera species in (A) Elles (Tunisia), (B) Bidart (France) and (C) Gamsbach (Austria). Thermocline dwelling globotruncanids (blue) are more abundant in the >150 μm fraction of Bidart and Gamsbach (open marine settings) as compared to Elles (neritic setting). Poor preservation of foraminifera in the 63–150 μm fraction of the Gamsbach section precluded quantitative analysis. (For interpretation of the references to color in this figure legend, the reader is referred to the web version of this article.)

dominance of thin-walled fragile heterohelicids in the assemblage (Fig. 10). In contrast, at Bidart the overall test fragmentation is quite low due to a high proportion of structurally more robust globotruncanids and quieter deposition at a greater depth. However, the proportion of leached out tests with holes due to dissolution increased (Fig. 10; red). At Gamsbach, the degree of fragmentation is

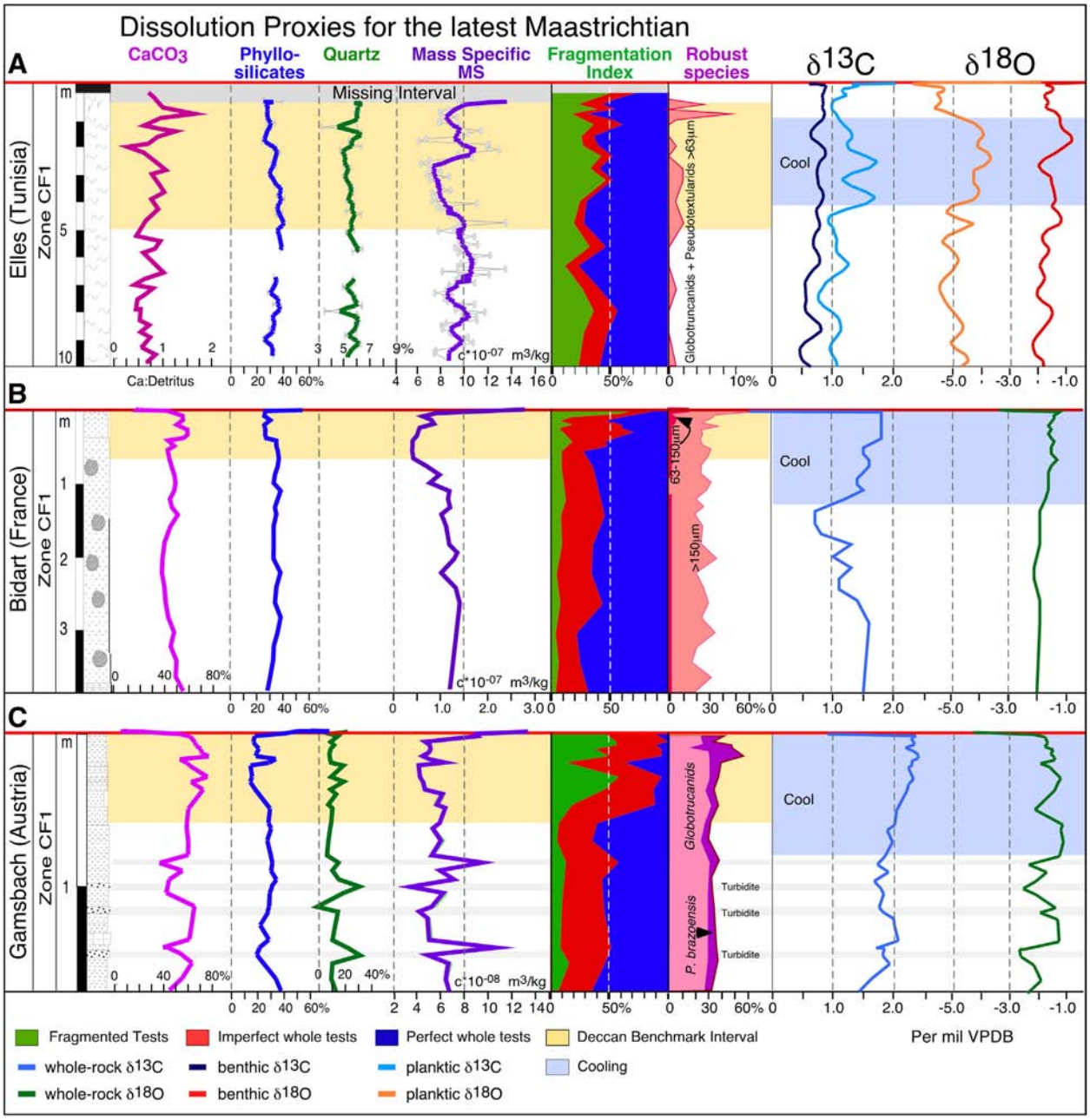

Fig. 10. Multi-proxy data shows a dissolution interval immediately preceding the KTB. A low magnetic susceptibility (MS) interval in the upper part of zone CF1 of Elles, Bidart and Gamsbach (yellow) marks a regional chemical benchmark of Deccan volcanism (after Font et al, 2011, 2014). Increased planktic foraminiferal test fragmentation in the low MS interval supports water column carbonate dissolution. (For interpretation of the references to color in this figure legend, the reader is referred to the web version of this article.)

high throughout zone CF1 despite a high abundance of globotruncanids. This can be attributed to the frequent turbiditic activity at this site that may have increased post-depositional transport and fragmentation. The variable lithology (deposition of quartz rich beds/lenses) may have facilitated pore-water dissolution, recrystallization-cementation leading to lithified sediments that are difficult to disaggregate and free individual tests.

8.5. Ocean acidification: the missing link to Deccan volcanism?

The main phase-2 of Deccan volcanism occurred over ~750kyr entirely within chron C29r, straddling the KTB (Schoene et al., 2014). However, all volcanism did not occur at uniform intensity within this interval, as inferred from the multiple eruptive events of geologically short duration separated by red/green boles indicating periods of quiescence (Subbarao et al., 2000; Chenet et al., 2007, 2008; Jay and Widdowson, 2008). Four of the Deccan phase-2 longest lava-flows across the Indian sub-continent (likely signifying peak volcanic activity) erupted within a duration of ~250 kyr (zone CF2–CF1) as seen in the Krishna–Godavari basin, India. The overlying Danian zone P1a sediments constrain the age of the KTB mass extinction as coincident with the final mega-flow of the peak phase-2 eruptions. (Keller et al., 2011a, 2012). The resultant cumulative loading of 12,000–28,000 Gigatons (Gt) of CO_2 into the end Cretaceous atmosphere within tens of thousand years could increase the pCO_2 on timescales that are recorded in the sediments. This excess CO_2 equilibrates with surface ocean water thus altering the carbonate chemistry. The carbonic acid (H_2CO_3) formed dissociates to bicarbonate anion (HCO^-_3) and H^+

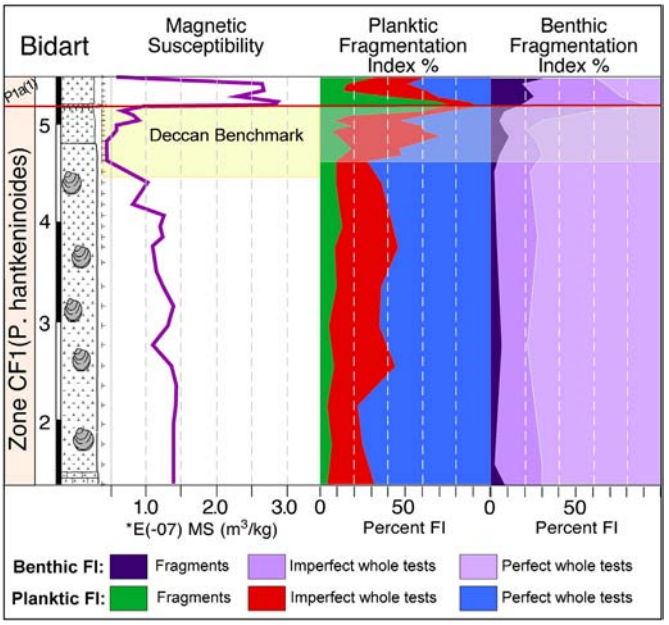

Fig. 11. Magnetic susceptibility (MS) data for Bidart (Font et al., 2011) along with the fragmentation index (FI) data for planktic and benthic foraminifera. The geochemical Deccan benchmark interval coincides with a pronounced water column dissolution event recorded by the planktic foraminifera. The benthic FI for the same interval indicate only a minor contribution of post-depositional breakage. (For interpretation of the references to color in this figure legend, the reader is referred to the web version of this article.)

ions, reducing the pH of surface waters. These H^+ ions combine with CO_3^{2-} anions forming more HCO_3^- and decreasing the bioavailability of CO_3^{2-} to calcifying organisms to build their tests.

The episodic release of hundreds to thousands of teragrams of volcanogenic SO_2 per year for each Deccan eruption would form sulfate aerosols upon reaction with atmospheric water vapor and precipitate out as toxic acid rain locally/regionally centennial timescales, shorter than the millennial timescales for removal of CO_2 (Self et al., 2008; Chenet et al., 2009; Mussard et al., 2014; Callegaro et al., 2014). This could have been directly toxic/lethal for continental flora and fauna of affected areas. On land, acid rain would exacerbate continental weathering. Sulfur dioxide would also lower the surface ocean pH further, significantly contributing to the calcification crisis and high-stress conditions for calcifying organisms on shorter timescales.

Ocean acidification has been identified as an important mechanism associated with faunal turnovers and mass extinction events through geological history (e.g. ocean anoxic events (OAEs) of the Paleozoic and the Paleocene–Eocene thermal maximum (PETM)) that have affected marine calcifiers e.g. coccolithophores, planktic and benthic foraminifera (review in Hönisch et al., 2012). Physiological manifestations of high-stress due to acidification recorded as dwarfism, deformed tests, and R-strategist-dominated assemblages in the Late Maastrichtian have already been linked with phase-2 Deccan volcanism (Erba et al., 2010; review in Punekar et al., 2014a). Moy et al. (2009) reported a 30%–35% lower calcification in modern *Globigerina bulloides* from the Southern Ocean as compared to Holocene specimens. The anthropogenic CO_2 emissions have resulted in acidification of the Southern Ocean in the past ~300 yr (drop in pH by 0.1 units, expected drop of 0.7 units in the next ~300 yr; Orr et al., 2005; Zeebe et al., 2008). Carbonate tests of planktic organisms can experience dissolution in the water column as demonstrated by the in vitro pteropod shell dissolution within 48 h of exposure to low pH waters (Fabry et al., 2008; Doney et al., 2009). The cumulative effect of thinner walled tests undergoing water-column dissolution can render a test increasingly fragile and vulnerable to fragmentation, consistent with our taphonomic evidence for ocean acidification.

There are multiple lines of evidence in support of global surface ocean acidification associated with the main phase-2 Deccan volcanism: (1) intensely corroded carbonate tests and rapid extinctions of Maastrichtian planktic foraminifera in the intertrappean sediments of the lava mega-flows in the Krishna–Godavari Basin of India (Keller et al., 2011a, 2012). (2) Strong carbonate dissolution and high-stress environments indicated by intense *Guembelitria* blooms (>95%) in CF1 of Meghalaya (NE India) (Gertsch et al., 2011). And (3) evidence for iron oxide dissolution by acidification inferred from low MS as well as for surface ocean acidification near the end of zone CF1 preceding the KTB at distal sites such as Bidart (France) and Gamsbach (Austria) as documented in this study.

9. Conclusions

Good temporal correlation between the age of the main phase of Deccan volcanic eruptions in India and the age and episodic nature of climate fluctuations worldwide has strengthened the case for large scale volcanism as a significant contributor to the Late Maastrichtian biotic stress that culminated in the KTB mass extinction. However, inherent limitations due to incompleteness of the stratigraphic record and the lack of a convincing kill-mechanism have inspired strong skepticism for this hypothesis.

A multi-proxy study of the Late Maastrichtian zone CF1 in Bidart (France) and Gamsbach (Austria) reveals events in the final ~160 ky of the Late Maastrichtian that are critical to understanding the role of Deccan volcanism in global high stress environments and leads to the following conclusions.

- The Late Maastrichtian warm event in the lower part of zone CF1 at Bidart (France) and Gamsbach (Austria) is recognized by faunal responses similar to those observed at Elles (Tunisia) and DSDP Site 525A.
- A period of low $\delta^{13}C$ values and decreased percent $CaCO_3$ content during the global warming may record a combination of increased continental ^{12}C influx through increased runoff, suppressed primary and calcifier productivity and equilibration of surface ocean waters with increased isotopically lighter volcanogenic CO_2.
- An increase in carbonate dissolution and foraminiferal test fragmentation suggests surface ocean acidification in 60-cm immediately preceding the KTB at Bidart (France) and Gamsbach (Austria). This event globally correlates with the low MS interval defined as the Deccan benchmark interval in Bidart by Font et al. (2011, 2014).
- The widespread ocean acidification interval is coincident with the rapid cooling. At Elles, evidence for another rapid warming following this interval coincides with the KTB mass extinction. The acidification may be the result of equilibration with huge amounts of CO_2 injected rapidly into the atmosphere at rates overwhelming the response time of feedback mechanisms.

Supplementary data to this article can be found online at http://dx.doi.org/10.1016/j.palaeo.2015.08.025.

Acknowledgments

This research was supported by Princeton University's Scott and Tuttle Funds, the U.S. National Science Foundation (grants NSF EAR-0207407, EAR-0447171 and EAR-1026271) and FCT (ref. PTDC/CTE-GIX/117298/2010). We thank the three anonymous reviewers and the Guest Editor Prof. Wolfram M. Kürschner for their insightful comments and suggestions.

References

Abrajevitch, A., Hori, R.S., Kodama, K., 2013. Rock magnetic record of the Triassic–Jurassic transition in pelagic bedded chert of the Inuyama section, Japan. Geology 41 (7), 803–806.

Abrajevitch, A., Font, E., Florindo, F., Roberts, A.P., 2015. Asteroid impact vs. Deccan eruptions: The origin of low magnetic susceptibility beds below the Cretaceous–Paleogene boundary revisited. Earth and Planetary Science Letters 430, 209–223.

Abramovich, S., Keller, G., 2002. High stress late Maastrichtian paleoenvironment: inference from planktonic foraminifera in Tunisia. Palaeogeogr. Palaeoclimatol. Palaeoecol. 178 (3), 145–164. http://dx.doi.org/10.1016/S0031-0182(01)00394-7.

Abramovich, S., Keller, G., 2003. Planktonic foraminiferal response to the latest Maastrichtian abrupt warm event: a case study from South Atlantic DSDP Site 525A. Mar. Micropaleontol. 48 (3), 225–249. http://dx.doi.org/10.1016/S0377-8398(03)00021-5.

Abramovich, S., Keller, G., Stüben, D., Berner, Z., 2003. Characterization of late Campanian and Maastrichtian planktonic foraminiferal depth habitats and vital activities based on stable isotopes. Palaeogeogr. Palaeoclimatol. Palaeoecol. 202 (1), 1–29. http://dx.doi.org/10.1016/S0031-0182(03)00572-8.

Abramovich, S., Yovel-Corem, S., Almogi-Labin, A., Benjamini, C., 2010. Global climate change and planktic formaminiferal response in the Maastrichtian. Paleoceanography 25, PA2201. http://dx.doi.org/10.1029/2009PA001843.

Abramovich, S., Keller, G., Berner, Z., Cymbalista, M., Rak, C., 2011. Maastrichtian planktic foraminiferal biostratigraphy and paleoenvironment of Brazos River, Falls County, Texas. In: Keller, G., Adatte, T. (Eds.), 100 SEPM Special Publication, pp. 123–156 http://dx.doi.org/10.1017/S0016756812001069.

Adatte, T., Stinnesbeck, W., Keller, G., 1996. Lithostratigraphic and mineralogic correlations of near K/T boundary sediments northeastern Mexico: implications for origin and nature of deposition. The Cretaceous–Tertiary Event and Other Catastrophes in Earth History, Boulder, Colorado. Geol. Soc. Am. Spec. Pap. 307, 211–226.

Alegret, L., Thomas, E., 2004. Benthic foraminifera and environmental turnover across the Cretaceous/Paleogene boundary at Blake Nose (ODP Hole 1049C, Northwestern Atlantic). Palaeogeogr. Palaeoclimatol. Palaeoecol. 208 (1), 59–83. http://dx.doi.org/10.1016/j.palaeo.2004.02.028.

Alegret, L., Molina, E., Thomas, E., 2001. Benthic foraminifera at the Cretaceous–Tertiary boundary around the Gulf of Mexico. Geology 29 (10), 891–894. http://dx.doi.org/10.1130/0091-7613(2001)029<0891:BFATCT>2.0.CO;2.

Alegret, L., Molina, E., Thomas, E., 2003. Benthic foraminiferal turnover across the Cretaceous/Paleogene boundary at Agost (southeastern Spain): paleoenvironmental inferences. Mar. Micropaleontol. 48 (3), 251–279. http://dx.doi.org/10.1016/S0377-8398(03)00022-7.

Alegret, L., Kaminski, M.A., Molina, E., 2004. Paleoenvironmental recovery after the Cretaceous/Paleogene boundary crisis: evidence from the marine Bidart section (SW France). Palaios 19 (6), 574–586. http://dx.doi.org/10.1669/0883-1351(2004)019<0574:PRATPB>2.0.CO;2.

Apellaniz, E., Baceta, J.I., Bernaola-Bilbao, G., Núñez-Betelu, K., Orúe-Etxebarría, X., Payros, A., Pujalte, V., Robin, E., Rocchia, R., 1997. Analysis of uppermost Cretaceous–lowermost Tertiary hemipelagic successions in the Basque Country (western Pyrenees): evidence for a sudden extinction of more than half planktic foraminifer species at the K/T boundary. Bull. Soc. Geol. Fr. 168, 783–793.

Arenillas, I., Arz, J., Molina, E., 2004. A new high-resolution planktic foraminiferal zonation and subzonation for the lower Danian. Lethaia 37 (1), 79–95. http://dx.doi.org/10.1080/00241160310005097.

Arz, J.A., Arenillas, I., 1998. Extinción en masa catastrófica de foraminíferos planctónicos en el límite Cretácico/Terciario del Pirineo occidental (España). Soc. Mex. Paleontol. Rev. 8 (2), 146–162. http://dx.doi.org/10.1155/2013/643278.

Arz, J.A., Molina, E., 2002. Late Campanian and Maastrichtian biostratigraphy and chronostratigraphy based on planktic foraminifera in temperate and subtropical latitudes (Spain, France and Tunisia). N. Jb. Geol. Paläont. (Abh.) 224 (2), 161–195.

Berger, W.H., Bonneau, M.C., Parker, F.L., 1982. Foraminifera on the deep-sea floor-lysocline and dissolution rate. Oceanol. Acta 5 (2), 249–258.

Bonté, P., Delacotte, O., Renard, M., Laj, C., Boclet, D., Jehanno, C., Rocchia, R., 1984. An iridium rich layer at the Cretaceous/Tertiary boundary in the Bidart section (southern France). Geophys. Res. Lett. 11 (5), 473–476. http://dx.doi.org/10.1029/GL011i005p00473.

Callegaro, S., Baker, D.R., De Min, A., Marzoli, A., Geraki, K., Bertrand, H., Viti, C., Nestola, F., 2014. Microanalyses link sulfur from large igneous provinces and Mesozoic mass extinctions. Geology 42 (10), 895–898. http://dx.doi.org/10.1130/G35983.1.

Chenet, A.-L., Quidelleur, X., Fluteau, F., Courtillot, V., Bajpai, S., 2007. 40 K–40Ar dating of the Main Deccan large igneous province: further evidence of KTB age and short duration. Earth Planet. Sci. Lett. 263 (1–2), 1–15. http://dx.doi.org/10.1016/j.epsl.2007.07.011.

Chenet, A.-L., Fluteau, F., Courtillot, V., Gérard, M., Subbarao, K.V., 2008. Determination of rapid Deccan eruptions across the Cretaceous–Tertiary boundary using paleomagnetic secular variation: results from a 1200-m-thick section in the Mahabaleshwar escarpment. J. Geophys. Res. 113 (B4). http://dx.doi.org/10.1029/2006JB004635.

Chenet, A.L., Courtillot, V., Fluteau, F., Gérard, M., Quidelleur, X., Khadri, S.F.R., Subbarao, K.V., Thordarson, T., 2009. Determination of rapid Deccan eruptions across the Cretaceous-Tertiary boundary using paleomagnetic secular variation: 2. Constraints from analysis of eight new sections and synthesis for a 3500-m-thick composite section. Journal of Geophysical Research: Solid Earth (1978–2012) 114, no. B6.

Clauser, S., 1994. Etudes stratigraphiques du Campanien et du Maastrichtien de l'Europe Occidentale: Cote Basque, Charentes (France), Limbourg (Pays-Bas). Documents du Bureau de Recherches Géologiques et Minières 235 p. 243.

Coccioni, R., Marsili, A., 2007. The response of benthic foraminifera to the K–Pg boundary biotic crisis at Elles (northwestern Tunisia). Palaeogeogr. Palaeoclimatol. Palaeoecol. 255 (1), 157–180. http://dx.doi.org/10.1016/j.palaeo.2007.02.046.

Delacotte, O., 1982. Etude magnétostratigraphique et géochimique de la limite Crétacé–Tertiaire de la coupe de Bidart (Pyrennées Atlantiques) PhD thesis Université Pierre et Marie Curie, Paris, France.

Doney, S.C., Fabry, V.J., Feely, R.A., Kleypas, J.A., 2009. Ocean acidifi cation: the other CO2 problem. Ann. Rev. Mar. Sci. 1, 169–192. http://dx.doi.org/10.1146/annurev.marine.010908.163834.

Egger, H., Rögl, F., Wagreich, M., 2004. Biostratigraphy and facies of Paleogene deep-water deposits at Gams (Gosau Group, Austria). Ann. Naturhist. Mus. Wien 106A, 281–307.

Egger, H., Koeberl, C., Wagreich, M., Stradner, H., 2009. The Cretaceous–Paleogene (K/Pg) boundary at Gams, Austria: nannoplankton stratigraphy and geochemistry of a bathyal northwestern Tethyan setting. Stratigraphy 6 (4), 333–347.

Ellwood, B., MacDonald, W., Wheeler, C., Benoist, S., 2003. The K–T boundary in Oman: identified using magnetic susceptibility field measurements with geochemical confirmation. Earth Planet. Sci. Lett. 206 (3), 529–540. http://dx.doi.org/10.1016/j.palaeo.2008.01.005.

Ellwood, B., Tomkin, J., Ratcliffe, K., Wright, M., Kafafy, A., 2008. High-resolution magnetic susceptibility and geochemistry for the Cenomanian/Turonian boundary GSSP with correlation to time equivalent core. Palaeogeogr. Palaeoclimatol. Palaeoecol. 261 (1), 105–126. http://dx.doi.org/10.1016/j.palaeo.2008.01.005.

Erba, E., Bottini, C., Weissert, H.J., Keller, C.E., 2010. Calcareous nannoplankton response to surface-water acidification around oceanic anoxic event 1a. Science 329 (5990), 428–432. http://dx.doi.org/10.1126/science.1188886.

Erbacher, J., Mosher, D.C., Malone, M.J., 2004. Demerara Rise: Equatorial Cretaceous and Paleogene Paleoceanographic Transect, Western Atlantic. Proceedings of the Ocean Drilling Program, Initial Reports, p. 207.

Fabry, V.J., Seibel, B.A., Feely, R.A., Orr, J.C., 2008. Impacts of ocean acidification on marine fauna and ecosystem processes. ICES J. Mar. Sci. J. Cons. 65 (3), 414–432. http://dx.doi.org/10.1093/icesjms/fsn048.

Font, E., Abrajevitch, A., 2014. Paleoenvironmental signature of the Deccan Phase 2. Front. Earth Sci. http://dx.doi.org/10.3389/feart.2014.0002.

Font, E., Nedelec, A., Ellwood, B.B., Mirao, J., Silva, P.F., 2011. A new sedimentary benchmark for the Deccan Traps volcanism? Geophys. Res. Lett. 38, L24309. http://dx.doi.org/10.1029/2011GL049824.

Font, E., Fabre, S., Nédélec, A., Adatte, T., Keller, G., Veiga-Pires, C., Ponte, J., Mirão, J., Khozyem, H., Spangenberg, J.E., 2014. Atmospheric halogen and acid rains during the main phase of Deccan eruptions: magnetic and mineral evidence. Geol. Soc. Am. Spec. Pap. 505, SPE505–SPE518. http://dx.doi.org/10.1130/2014.2505(18).

Galbrun, B., Gardin, S., 2004. New chronostratigraphy of the Cretaceous–Paleogene boundary interval at Bidart (France). Earth Planet. Sci. Lett. 224, 19–32. http://dx.doi.org/10.1016/j.epsl.2004.04.043.

Gallala, N., 2013. Planktonic foraminiferal biostratigraphy and correlation across the Cretaceous–Paleogene Transition at the Tethyan and the Atlantic Realms. Paleontol. J. 2013.

Gallala, N., Zaghbib-Turki, D., Arenillas, I., Arz, J.A., Molina, E., 2009. Catastrophic mass extinction and assemblage evolution in planktic foraminifera across the Cretaceous/Paleogene (K/Pg) boundary at Bidart (SW France). Mar. Micropaleontol. 72 (3), 196–209. http://dx.doi.org/10.1016/j.marmicro.2009.05.001.

Gardin, S., 2002. Late Maastrichtian to early Danian calcareous nannofossils at Elles (Northwest Tunisia). A tale of one million years across the K–T boundary. Palaeogeogr. Palaeoclimatol. Palaeoecol. 178 (3), 211–231.

Georgescu, M.D., Abramovich, S., 2009. A new Late Cretaceous (Maastrichtian) serial planktic foraminifer (Family Heterohelicidae) with early planispiral coil and revision of *Spiroplecta* Ehrenberg, 1844. Geobios 42 (6), 687–698.

Gertsch, B., Keller, G., Adatte, T., Garg, R., Prasad, V., Berner, Z., Fleitmann, D., 2011. Environmental effects of Deccan volcanism across the Cretaceous–Tertiary transition in Meghalaya, India. Earth Planet. Sci. Lett. 310 (3–4), 272–285. http://dx.doi.org/10.1016/j.epsl.2011.08.015.

Gorostidi, A., Lamolda, M.A., 1995. La nannoflora calcárea y el tránsito KT de la sección de Bidart (SW de Francia). Revista Española de Paleontología no. Homenaje al Dr. Guillermo Colompp. 153–168.

Grachev, A.F. (Ed.), 2009. The K/T boundary of Gams (Eastern Alps, Austria) and the nature of terminal Cretaceous mass extinction. Geologische Bundesanstalt, Vienna, p. 199 http://dx.doi.org/10.2205/2009-GAMSbook.

Grachev, A.F., Korchagin, O.A., Kollmann, H.A., Pechersky, D.M., Tsel 'movich, V.A., 2005. A new look at the nature of the transitional layer at the K/T boundary near Gams, Eastern Alps, Austria, and the problem of the mass extinction of the biota. Russ. J. Earth Sci. 7. http://dx.doi.org/10.2205/2005ES000189.

Grachev, A.F., Borisovsky, S.E., Grigor'eva, A.V., 2008. The first find of native rhenium in the transitional clay layer at the Cretaceous/Paleogene boundary in the Gams Section (eastern Alps, Austria). Doklady Earth Sciences 422(1). MAIK Nauka/Interperiodica, pp. 1065–1067. http://dx.doi.org/10.1134/S1028334X08070131.

Gradstein, F., Ogg, J., Smith, A., 2004. A Geologic Time Scale 2004. Cambridge University Press, Cambridge, p. 589.

Haslett, S.K., 1994. Planktonic foraminiferal biostratigraphy and palaeoceanography of the Cretaceous–Tertiary boundary section at Bidart, south-west France. Cretac. Res. 15, 179–192. http://dx.doi.org/10.1006/cres.1994.1009.

Haq, B.U., 1988. "Mesozoic and Cenozoic chronostratigraphy and cycles of sea-level change." SEPM Special Publications v. 42.

Haubold, H., Scholger, R., Frisch, W., Summesberger, H., Mauritsch, H.J., 1999. Reconstruction of the geodynamic evolution of the Northern Calcareous Alps by means of paleomagnetism. Phys. Chem. Earth Solid Earth Geod. A 24, 697–703. http://dx.doi.org/10.1016/S1464-1895(99)00101-5.

Hönisch, B., Ridgwell, A., Schmidt, D.N., Thomas, E., Gibbs, S.J., Sluijs, A., Zeebe, R., Kump, L., Martindale, R.C., Greene, S.E., Kiessling, G., Ries, J., Zachos, J.C., Royer, D.L., Barker, S., Marchitto Jr., T.M., Moyer, R., Pelejero, C., Ziveri1, P., Foster, G.L., Williams, B., 2012. The geological record of ocean acidifi cation. Science 335 (6072), 1058–1063. http://dx.doi.org/10.1126/science.1208277.

Jay, A.E., Widdowson, M., 2008. Stratigraphy, structure and volcanology of the SE Deccan continental flood basalt province: implications for eruptive extent and volumes. J. Geol. Soc. 165 (1), 177–188. http://dx.doi.org/10.1144/0016-76492006-062.

Keller, G., 2003. Guembelitria-dominated late Maastrichtian planktic foraminiferal assemblages mimic early Danian in central Egypt. Marine Micropaleontology 47 (1), 71–99.

Please cite this article as: Punekar, J., et al., A multi-proxy approach to decode the end-Cretaceous mass extinction, Palaeogeogr. Palaeoclimatol. Palaeoecol. (2015), http://dx.doi.org/10.1016/j.palaeo.2015.08.025

Keller, G., 2004. Low-diversity, late Maastrichtian and early Danian planktic foraminiferal assemblages of the eastern Tethys. J. Foraminifer. Res. 34 (1), 49–73.

Keller, G., Benjamini, C., 1991. Paleoenvironment of the eastern Tethys in the early Danian. Palaios 6, 439–464. http://dx.doi.org/10.2307/3514984.

Keller, G., Pardo, A., 2004. Age and paleoenvironment of the Cenomanian–Turonian global stratotype section and point at Pueblo. Colorado. Marine Micropaleontology 51 (1), 95–128.

Keller, G., Li, L., MacLeod, N., 1995. The Cretaceous/Tertiary boundary stratotype section at El Kef, Tunisia: how catastrophic was the mass extinction? Palaeogeogr. Palaeoclimatol. Palaeoecol. 119, 221–254. http://dx.doi.org/10.1016/0031-0182(95)00009-7.

Keller, G., Adatte, T., Stinnesbeck, W., Stüben, D., Kramar, U., Berner, Z., Li, L., Perch-Nielsen, K.V.S., 1997. The Cretaceous–Tertiary transition on the shallow Saharan platform of southern Tunisia. Geobios 30 (7), 951–975.

Keller, G., Adatte, T., Burns, S.J., Tantawy, A.A., 2002a. High-stress paleoenvironment during the late Maastrichtian to early Paleocene in central Egypt. Palaeogeogr. Palaeoclimatol. Palaeoecol. 187, 35e60. http://dx.doi.org/10.1016/S0031-0182(02)00504-7.

Keller, G., Adatte, T., Stinnesbeck, W., Luciani, V., Karoui, N., Zaghbib-Turki, D., 2002b. Paleoecology of the Cretaceous–Tertiary mass extinction in planktic foraminifera. Palaeogeogr. Palaeoclimatol. Palaeoecol. 178, 257–298. http://dx.doi.org/10.1016/S0031-0182(01)00399-6.

Keller, G., Stinnesbeck, W., Adatte, T., Stüben, D., 2003. Multiple Impacts across the Cretaceous–Tertiary boundary. Earth-Sci. Rev. 62, 327–363. http://dx.doi.org/10.1016/S0012-8252(02)00162-9.

Keller, G., Abramovich, S., Adatte, T., Berner, Z., 2011a. Biostratigraphy, age of the Chicxulub impact, and depositional environment of the Brazos River KTB sequences. In: Keller, G., Adatte, T. (Eds.), The End-Cretaceous Mass Extinction and the Chicxulub Impact in Texas: Society for Sedimentary Geology (SEPM) Special Publication 100, pp. 81–122.

Keller, G., Bhowmick, P.K., Upadhyay, H., Dave, A., Reddy, A.N., Jaiprakash, B.C., Adatte, T., 2011b. Deccan volcanism linked to the Cretaceous–Tertiary boundary mass extinction: new evidence from ONGC Wells in the Krishna–Godavari Basin. J. Geol. Soc. India 78, 399–428. http://dx.doi.org/10.1007/s12594-011-0107-3.

Keller, G., Adatte, T., Bhowmick, P.K., Upadhyay, H., Dave, A., Reddy, A.N., Jaiprakash, B.C., 2012. Nature and timing of extinctions in Cretaceous–Tertiary planktic foraminifera preserved in Deccan intertrappean sediments of the Krishna–Godavari Basin, India. Earth Planet. Sci. Lett. 341, 211–221. http://dx.doi.org/10.1016/j.epsl.2012.06.021.

Keller, G., Khozyem, H., Adatte, T., Malarkodi, N., Spangenberg, J.E., Stinnesbeck, W., 2013. Chicxulub impact spherules in the North Atlantic and Caribbean: age constraints and Cretaceous–Tertiary boundary hiatus. Geol. Mag. 150 (05), 885–907.

Le, J., Shackleton, N.J., 1992. Carbonate dissolution fluctuations in the western equatorial Pacific during the late Quaternary. Paleoceanography 7 (1), 21–42.

Li, L., Keller, G., 1998a. Maastrichtian climate, productivity and faunal turnovers in planktic foraminifera in South Atlantic DSDP Sites 525A and 21. Mar. Micropaleontol. 33, 55–86. http://dx.doi.org/10.1016/S0377-8398(97)00027-3.

Li, L., Keller, G., 1998b. Diversification and extinction in Campanian–Maastrichtian planktic foraminifera of northwestern Tunisia. Eclogae Geol. Helv. 91, 75–102 (doi: 0012-9402/98/010075-28).

Li, L., Keller, G., Stinnesbeck, W., 1999. The Late Campanian and Maastrichtian in northwestern Tunisia: palaeoenvironmental inferences from lithology, macrofauna and benthic foraminifera. Cretaceous Research 20 (2), 231–252.

MacLeod, N., Keller, G., 1991. Hiatus distributions and mass extinctions at the Cretaceous/Tertiary boundary. Geology 19, 497–501. http://dx.doi.org/10.1016/0031-0182(95)00009-7.

Malmgren, B.A., 1987. Differential dissolution of Upper Cretaceous planktonic foraminifera from a temperate region of the South Atlantic Ocean. Mar. Micropaleontol. 11 (4), 251–271.

Mary, C., Moreau, M.G., Orue-Etxebarria, X., Apellaniz, E., Courtillot, V., 1991. Biostratigraphy and magnetostratigraphy of the Cretaceous/Tertiary Sopelana section (Basque country). Earth and Planetary Science Letters 106 (1), 133–150.

Moore, J.C., Klaus, A., Bangs, N.L., 1998. Site 1049, Proc. ODP, Initial Reports 171A, pp. 47–91.

Moy, A.D., Howard, W.R., Bray, S.G., Trull, T.W., 2009. Reduced calcification in modern Southern Ocean planktonic foraminifera. Nat. Geosci. 2 (4), 276–280. http://dx.doi.org/10.1038/ngeo460.

Mussard, M., Le Hir, G., Fluteau, F., Lefebvre, V., Goddéris, Y., 2014. Modeling the carbon-sulfate interplays in climate changesrelated to the emplacement of continental flood basalts. In: Keller, G., Kerr, A.C. (Eds.), Volcanism, Impacts, and Mass Extinctions: Causes and Effects. Geological Society of America Special Paper 505. http://dx.doi.org/10.1130/2014.2505(17).

Nederbragt, A.J., 1991. Late Cretaceous biostratigraphy and development of Heterohelicidae (planktic foraminifera). Micropaleontology 329–372 http://dx.doi.org/10.2307/1485910.

Nelson, B.K., Macleod, G.K., Ward, P.D., 1991. Rapid change in strontium isotopic composition of seawater before the Cretaceous/Tertiary boundary. Nature 351, 644–647. http://dx.doi.org/10.1038/351644a0.

Olsson, R.K., Hemleben, C., Berggren, W.A., Huber, B.T., 1999. Atlas of Paleocene Planktonic Foraminifera. Smithsonian Contribution to Paleobiology No. 85. Smithsonian Institution Press, Washington D.C., p. 252.

Orr, J.C., Fabry, V.J., Aumont, O., Bopp, L., Doney, S.C., Feely, R.A., Gnanadesikan, A., Gruber, N., Ishida, A., Joos, F., Key, R.M., Lindsay, K., Maier-Reimer, E., Matear, R., Monfray, P., Mouchet, A., Najjar, R.G., Plattner, G.-K., Rodgers, K.B., Sabine, C.L., Sarmiento, J.L., Schlitzer, R., Slater, R.D., Totterdell, I.J., Weirig, M.-F., Yamanaka, Y., Yool, A., 2005. Anthropogenic ocean acidification over the twenty-first century and its impact on calcifying organisms. Nature 437, 681–686. http://dx.doi.org/10.1038/nature04095.

Pechersky, D.M., Grachev, A.F., Nourgaliev, D.K., Tsel'movich, V.A., Sharonova, Z.V., 2006. Magnetolithologic and magnetomineralogical characteristics of deposits at the Mesozoic/Cenozoic boundary: Gams section (Austria). Russ. J. Earth Sci. 8 (3). http://dx.doi.org/10.2205/2006ES000204.

Peybernes, B., Fondecave-Wallez, M.J., Gourinard, Y., Eichène, P., 1997. Stratigraphie séquentielle comparée et grade-datation par les foraminifères planctoniques du Campano-Maastrichtien et du Paléocène de quelques sites d'Europe sud-occidentale et d'Afrique du Nord. C. R. Acad. Sci. Ser. D Sci. Terre 324, 839–846. http://dx.doi.org/10.1016/S1251-8050(97)82519-0.

Pueyo, E.L., Mauritsch, H.J., Gawlick, H.-J., Scholger, R., Frisch, W., 2007. New evidence for block and thrust sheet rotations in the central northern Calcareous Alps deduced from two pervasive remagnetization events. Tectonics 26, TC5011. http://dx.doi.org/10.1029/2006TC001965.

Punekar, J., Keller, G., Khozyem, H., Hamming, C., Adatte, T., Tantawy, A.A., Spangenberg, J.E., 2014a. Late Maastrichtian–early Danian high-stress environments and delayed recovery linked to Deccan volcanism. Cretac. Res. 49, 63–82. http://dx.doi.org/10.1016/j.cretres.2014.01.002.

Punekar, J., Mateo, P., Keller, G., 2014b. Effects of Deccan volcanism on paleoenvironment and planktic foraminifera: a global survey. Geol. Soc. Am. Spec. Pap. 505, 91–116. http://dx.doi.org/10.1130/2014.2505(04).

Raja Rao, C.S., Sahasrabudhe, S.S., Deshmukh, S.S., Raman, R., 1999. Distribution, structure and petrography of the Deccan Traps, India. In: Subbarao, K.V. (Ed.)Deccan Volcanic Province, Memoir — Geological Society of India 43, pp. 401–414.

Razin, P., 1989. Evolution tectono-sédimentaire alpine des Pyrénées Basques à l'Ouest de la transformante de Pampelune (Province du Labourd) (Thèse de doctorat) Université de Bordeaux III, p. 464.

Renard, M., Delacotte, O., Létolle, R., 1982. Le strontium et les isotopes stables dans les carbonates totaux de quelques sites de l'Atlantique et de la Tethys. Bull. Soc. Geol. Fr. 14, 519–534. http://dx.doi.org/10.2113/gssgfbull.S7-XXIV.3.519.

Renne, P.R., Deino, A.L., Hilgen, F.J., Kuiper, K.F., Mark, D.F., Mitchell, W.S., Morgan, L.E., Mundil, R., Smit, J., 2013. Time scales of critical events around the Cretaceous – Paleogene boundary. Science 339 (6120), 684–687. http://dx.doi.org/10.1126/science.1230492.

Robaszynski, F., Caron, M., Gonzalez-Donoso, J.M., Wonders, A.H., Ewgpf 1983–1984. Paris Atlas of late Cretaceous Globotruncanids. Rev. Micropaléontol., 36 (3–4), 145–305.

Rocchia, R., Boclet, D., Bonté, Ph., Devineau, J., Jéhanno, C., Renard, M., 1987. Comparaison des distributions de l'iridium observéesàla limite Crétacé – Tertiaire dans divers sites européens. Mém. Soc. Géol. Fr. N.S. 150 (1987), 95–103.

Rocchia, R., Robin, E., Froget, L., Gayraud, J., 1996. Stratigraphic distribution of extraterrestrial markers at the Cretaceous–Tertiary boundary in the Gulf of Mexico area: implications for the temporal complexity of the event. Geol. Soc. Am. Spec. Pap. 307, 279–286.

Schöbel, S., de Wall, H., Ganerød, M., Pandit, M.K., Rolf, C., 2014. Magnetostratigraphy and 40Ar–39Ar geochronology of the Malwa Plateau region (Northern Deccan Traps), central western India: significance and correlation with the main Deccan Large Igneous Province sequences. J. Asian Earth Sci. 89, 28–45. http://dx.doi.org/10.1016/j.jseaes.2014.03.022.

Schoene, B., Samperton, K., Eddy, M., Keller, G., Adatte, T., Bowring, S., Khadri, S.F.R., Gertsch, B., 2014. U – Pb geochronology of the Deccan Traps and relation to the end-Cretaceous mass extinction. Science http://dx.doi.org/10.1126/science.aaa0118 (aaa0118).

Self, S., Blake, S., Sharma, K., Widdowson, M., Sephton, S., 2008. Sulfur and chlorine in Late Cretaceous Deccan magmas and eruptive gas release. Science 319, 1654–1657. http://dx.doi.org/10.1126/science.1152830.

Seyve, C., 1984. Le passage Crétacé–Tertiaire à Pont Labau. Bull. Centres Rech. Explor. Prod. Elf-Aquitaine 8, 385–423.

Seyve, C., 1990. Nannofossil biostratigraphy of the Cretaceous-Tertiary boundary in the French Basque Country. Bulletin des Centres de Recherches Exploration-Production Elf Aquitaine 14 (2), 553–572.

Shackleton, N., Boersma, A., 1985. History of the Walvis Ridge. A précis of the results of DSDP Leg 74. In: Moore, T.C. Jr, Rabinowitz, P.D., Borella, P.E. (Eds.), South Atlantic, Paleoceanography 57.

Smit, J., ten Kate, W.G.H.Z., 1982. Trace-element patterns at the Cretaceous–Tertiary boundary-consequences of a large impact. Cretac. Res. 3, 307–332.

Stüben, D., Kramar, U., Berner, Z.A., Meudt, M., Keller, G., Abramovich, S., Adatte, T., Hambach, U., Stinnesbeck, W., 2003. Late Maastrichtian paleoclimatic and paleoceanographic changes inferred from Sr/Ca ratio and stable isotopes. Palaeogeogr. Palaeoclimatol. Palaeoecol. 199 (1), 107–127. http://dx.doi.org/10.1016/S0031-0182(03)00499-1.

Subbarao, K.V., Bodas, M.S., Khadri, S.F.R., Beane, J.E., 2000. Penrose Deccan 2000, Field Excursion Guide to the Western Deccan Basalt Province. Penrose Field Guides, B. Geological Society of India, ed.

Summesberger, H., Wagreich, M., Bryda, G., 2009. Upper Maastrichtian cephalopods and the correlation to calcareous nannoplankton and planktic foraminifera zones in the Gams Basin (Gosau Group; Styria, Austria). Ann. Naturhist. Mus. Wien 111A, 159–182.

Tantawy, A.A., Keller, G., Pardo, A., 2009. Late Maastrichtian volcanism in the Indian Ocean: effects on calcareous nannofossils and planktic foraminifera. Palaeogeogr. Palaeoclimatol. Palaeoecol. 284 (1), 63–87. http://dx.doi.org/10.1016/j.palaeo.2009.08.025.

Thibault, N., Gardin, S., 2007. The late Maastrichtian nannofossil record of climate change in the South Atlantic DSDP Hole 525A. Marine Micropaleontology 65 (3), 163–184.

Thibault, N., Gardin, S., 2010. The calcareous nannofossil response to the end-Cretaceous warm event in the Tropical Pacific. Palaeogeogr. Palaeoclimatol. Palaeoecol. 291 (3), 239–252. http://dx.doi.org/10.1016/j.palaeo.2010.02.036.

Thibault, N., Husson, D., 2015. "Climatic fluctuations and sea-surface water circulation patterns at the end of the Cretaceous era: Calcareous nannofossil evidence.". Palaeogeography, Palaeoclimatology, Palaeoecology http://dx.doi.org/10.1016/j.palaeo.2015.07.049 (in press).

Thibault, N., Minoletti, F., Gardin, S., Renard, M., 2004. Morphométrie de nannofossiles calcaires au passage Crétacé–Paléocène des coupes de Bidart (France) et d'Elles

Please cite this article as: Punekar, J., et al., A multi-proxy approach to decode the end-Cretaceous mass extinction, Palaeogeogr. Palaeoclimatol. Palaeoecol. (2015), http://dx.doi.org/10.1016/j.palaeo.2015.08.025

(Tunisie). Comparaison avec les isotopes stables du carbone et de l'oxygène. Bull. Soc. Geol. Fr. 175.
Thunell, R.C., 1976. Optimum indices of calcium carbonate dissolution, in deep-sea sediments. Geology 4 (9), 525–528.
Vonhof, H.B., Smit, J., 1997. High-resolution late Maastrichtian–early Danian oceanic $^{87}Sr/^{86}Sr$ record: implications for Cretaceous–Tertiary boundary events. Geology 25, 347–350. http://dx.doi.org/10.1130/0091-7613(1997)025<0347:HRLMED>2.3.CO;2.
Wagreich, M., 1993. Subcrustal tectonic erosion in orogenic belts — a model for the Late Cretaceous subsidence of the Northern Calcareous Alps (Austria). Geology 21, 941–944.
Wagreich, M., 1995. Subduction tectonic erosion and Late Cretaceous subsidence along the northern Austroalpine margin (Eastern Alps, Austria). Tectonophysics 242, 63–78.
Wagreich, M., Krenmayr, H.-G., 1993. Nannofossil biostratigraphy of the Late Cretaceous Nierental Formation, Northern Calcareous Alps (Bavaria, Austria). Zitteliana 20, 67–77.
Wagreich, M., Krenmayr, H.-G., 2005. Upper Cretaceous oceanic red beds (CORB) in the Northern Calcareous Alps (Nierental Formation, Austria): slope topography and clastic input as primary controlling factors. Cretac. Res. 26, 57–64.
Widmark, J.G.V., Malmgren, B.A., 1992. Benthic foraminiferal changes across the Cretaceous/Tertiary boundary in the deep sea; DSDP sites 525, 527, and 465. J. Foram. Res. 22 (2), 81–113.
Williams, D.F., Healy-Williams, N., Laschak, P., 1985. Dissolution and water-mass patterns in the southeast Indian Ocean, I, Evidence from Recent to late Holocene foraminiferal assemblages. Geol. Soc. Am. Bull. 96, 176–189.
White, A.F., Peterson, M.L., Hochella, M.F., 1994. Electrochemistry and dissolution kinetics of magnetite and ilmenite. Geochimica et Cosmochimica Acta 58 (8), 1859–1875.
Zeebe, R.E., 2012. History of seawater carbonate chemistry, atmospheric CO_2, and ocean acidification. Annu. Rev. Earth Planet. Sci. 40, 141–165. http://dx.doi.org/10.1146/annurev-earth-042711-105521.
Zeebe, R.E., Zachos, J.C., Caldeira, K., Tyrrell, T., 2008. Carbon emissions and acidification. Science 321, 51–52. http://dx.doi.org/10.1126/science.1159124.

Please cite this article as: Punekar, J., et al., A multi-proxy approach to decode the end-Cretaceous mass extinction, Palaeogeogr. Palaeoclimatol. Palaeoecol. (2015), http://dx.doi.org/10.1016/j.palaeo.2015.08.025